



**HAL**  
open science

## Harsh intertidal environment enhances metabolism and immunity in oyster (*Crassostrea gigas*) spat

Charlotte Corporeau, Sébastien Petton, Romain Vilaça, Lizenn Delisle, Claudie Quéré, Valérian Le Roy, Christine Dubreuil, Sandra Lacas-Gervais, Yann Guitton, Sébastien Artigaud, et al.

### ► To cite this version:

Charlotte Corporeau, Sébastien Petton, Romain Vilaça, Lizenn Delisle, Claudie Quéré, et al.. Harsh intertidal environment enhances metabolism and immunity in oyster (*Crassostrea gigas*) spat. *Marine Environmental Research*, 2022, 180, pp.105709. 10.1016/j.marenvres.2022.105709 . hal-03858249

**HAL Id: hal-03858249**

**<https://hal.science/hal-03858249>**

Submitted on 28 Nov 2022

**HAL** is a multi-disciplinary open access archive for the deposit and dissemination of scientific research documents, whether they are published or not. The documents may come from teaching and research institutions in France or abroad, or from public or private research centers.

L'archive ouverte pluridisciplinaire **HAL**, est destinée au dépôt et à la diffusion de documents scientifiques de niveau recherche, publiés ou non, émanant des établissements d'enseignement et de recherche français ou étrangers, des laboratoires publics ou privés.

1 **Title: Harsh intertidal environment enhances metabolism and immunity in oyster**  
2 **(*Crassostrea gigas*) spat.**

3 **Running title: Intertidal environment improves oyster health.**

4 Charlotte Corporeau<sup>1\*</sup>, Sébastien Petton<sup>1</sup>, Romain Vilaça<sup>1</sup>, Lizenn Delisle<sup>1,2</sup>, Claudie Quéré<sup>1</sup>,  
5 Valérien Le Roy<sup>1</sup>, Christine Dubreuil<sup>1</sup>, Sandra Lacas-Gervais<sup>3</sup>, Yann Guitton<sup>4</sup>, Sébastien  
6 Artigaud<sup>1</sup>, Benoît Bernay<sup>5</sup>, Vianney Pichereau<sup>1</sup>, Arnaud Huvet<sup>1</sup>, Bruno Petton<sup>1</sup>, Fabrice  
7 Pernet<sup>1</sup>, Elodie Fleury<sup>1</sup>, Stéphanie Madec<sup>1</sup>, Christophe Brigaudeau<sup>6</sup>, Catherine Brenner<sup>7</sup> and  
8 Nathalie M. Mazure<sup>8</sup>.

9 <sup>1</sup> Ifremer, Univ. Bretagne Occidentale, CNRS, IRD, Équipe soutenue par la fondation ARC,  
10 UMR 6539, LEMAR, F- 29280, Plouzané, France

11 <sup>2</sup> Present adress : Cawthron Institute, Animal health team, Aquaculture Group, Private Bag 2,  
12 Nelson 7042, New Zealand.

13 <sup>3</sup> Université Côte d'Azur, Centre Commun de Microscopie Appliquée, CCMA, Nice, France.

14 <sup>4</sup> Laboratoire d'étude des Résidus et Contaminants dans les Aliments, Oniris, INRA, F-44307  
15 Nantes, France.

16 <sup>5</sup> Plateforme Proteogen, SFR ICORE 4206, Univ. Caen Basse-Normandie, 14000 Caen,  
17 France.

18 <sup>6</sup> Inserm U1227, Univ. Bretagne Occidentale, 2 bis avenue Foch, 29200 Brest, France

19 <sup>7</sup> Université Paris-Saclay, CNRS, Institut Gustave Roussy, Aspects métaboliques et  
20 systémiques de l'oncogénèse pour de nouvelles approches thérapeutiques, 94805, Villejuif,  
21 France.

22 <sup>8</sup> Inserm U1065, Centre Méditerranéen de Médecine Moléculaire, 151 route St Antoine de  
23 Ginestière, 06204 Nice, France.

24 \*corresponding author's email address: charlotte.corporeau@ifremer.fr

25 **Keywords:** environment, marine invertebrate, metabolism, OsHV-1.

## 26 **Highlights**

27 The metabolism and immunity of oysters are modified as a function of their habitat.

28 Increasing oysters' bathymetry is an advantage against pathogens in the field.

29 An intertidal footprint in oysters is detected at the proteomic level.

## 30 **ABSTRACT**

31 The Pacific oyster *Crassostrea gigas* is established in the marine intertidal zone, experiencing  
32 rapid and highly dynamic environmental changes throughout the tidal cycle. Depending on  
33 the bathymetry, oysters face oxygen deprivation, lack of nutrients, and high changes in  
34 temperature during alternation of the cycles of emersion/immersion. Here we showed that  
35 intertidal oysters at a bathymetry level of 3 and 5 meters delayed by ten days the onset of  
36 mortality associated with Pacific Oyster Mortality Syndrome (POMS) as compared to subtidal  
37 oysters. Intertidal oysters presented a lower growth but similar energetic reserves to subtidal  
38 oysters but induced proteomic changes indicative of a boost in metabolism, inflammation, and  
39 innate immunity that may have improved their resistance during infection with the Ostreid  
40 herpes virus. Our work highlights that intertidal harsh environmental conditions modify host-  
41 pathogen interaction and improve oyster health. This study opens new perspectives on oyster  
42 farming for mitigation strategies based on tidal height.

## 43 **1. INTRODUCTION**

44 The Pacific oyster *Crassostrea gigas* (*C. gigas*) is a sessile estuarine bivalve living in the  
45 coastal zone. *C. gigas* constitutes a great model species able to support rapid and dynamic  
46 environmental changes. Intertidal oysters are daily exposed to rapid changes in the food  
47 supply, oxygen, salinity, pH, and temperature conditions, throughout the tidal cycle  
48 depending on their bathymetric level (Li et al., 2018; Scanes et al., 2017; Zhang et al., 2016,  
49 2012). *C. gigas* endures temperatures ranging from below zero to 49°C, salinities from 10 up  
50 to 35 ppm and is particularly well adapted to anoxia during prolonged air exposure as well as  
51 rapid and long-term hypoxia (0.1% O<sub>2</sub>; weeks to months) (Bayne, 2017; Donaghy et al., 2013;  
52 Falfushynska et al., 2020; Guévelou et al., 2013; Sussarellu et al., 2013, 2012). In contrast to  
53 vertebrates, *C. gigas* presents an exceptional mitochondrial resilience to temperature, salinity,  
54 hypoxia (Sokolova, 2018), and extreme tolerance to hypoxia was related to mitochondria  
55 plasticity ability to maintain respiratory capacity in response to oxygen loss (Donaghy et al.,  
56 2013; Sokolov et al., 2019; Sussarellu et al., 2013, 2012). *C. gigas* can survive fasting for  
57 more than 6 months at 14°C (Whyte et al., 1990) and continue sexual maturation under  
58 complete food deprivation at 18°C (Rozenn Cannuel, 2005). *C. gigas* possesses unique  
59 molecular features to respond to environmental changes in its intertidal stressful habitat,

60 based on a combination of strong cellular homeostasis control, a large number of chaperone  
61 heat-shock hsp70 genes (88), and several copies of anti-oxidant enzymes (Zhang et al., 2016,  
62 2012). The intertidal Pacific oyster is therefore a good model species to study the interaction  
63 between physical traits of a stressful intertidal environment and biological regulation of  
64 cellular energetic metabolism.

65 Since 2008, spat oysters are dying in most rearing areas in the world. Mortality results from a  
66 Pacific Oyster Mortality Syndrome (POMS) caused by the Ostreid Herpes Virus-1 (OsHV-1)  
67 infection and followed by fatal bacteremia (de Lorgeril et al., 2018). OsHV-1 replicates in  
68 oyster circulating immune cells (hemocytes) which induces an immune depression and  
69 subsequent bacterial colonization leading to death (de Lorgeril et al., 2018; Morga et al.,  
70 2017). Oyster metabolism is a key component of POMS since the energy metabolism is  
71 hijacked by OsHV-1 for its replication, as the viral appropriation of host-cell biomaterials.  
72 Indeed, as shown in *C. gigas* larvae, OsHV-1 induces a metabolic reprogramming known as  
73 the Warburg effect (Corporeau et al., 2019, 2014; Rosani et al., 2019; Sanchez and Lagunoff,  
74 2015; Young et al., 2017). The Warburg effect could facilitate the creation of new OsHV-1  
75 viral particles in *C. gigas* during its replication phase, as demonstrated in *Paeneus japonicus*  
76 shrimp during infection by the white spot syndrome virus (WSSV) (Chen et al., 2011; Su et  
77 al., 2014). The Warburg effect is a metabolic reprogramming of cells producing large  
78 amounts of building blocks (DNA, lipids, amino acids) for division, which is one hallmark of  
79 proliferating cancer cells in vertebrates (Fouad and Aanei, 2017; Warburg, 1956).

80 Interestingly, increasing the bathymetry of oyster settlements decreases the mortality risk  
81 during an OsHV-1 outbreak (Azéma et al., 2017; Pernet et al., 2019) but mechanisms remain  
82 unknown. Here we deployed oysters in a farming area at Low (1.6 m; subtidal), Middle (3 m;  
83 intertidal), and High (5 m; intertidal) bathymetry corresponding to 3.9% (subtidal), 42.8%,  
84 and 55.1% (intertidal) emersion time, respectively. We monitored local temperature in the bag  
85 and analyzed the physiological responses of oysters during OsHV-1-associated mortality as a  
86 function of the bathymetry. We analyzed the impact of bathymetry on oyster physiology by  
87 using “omics” technologies (proteomics and metabolomics) referenced as emergent tools for  
88 the study of host-pathogen interaction in bivalves and to identify bioindicators of animal  
89 health (Alfaro and Young, 2018; Rosani et al., 2019). To identify any changes in interaction  
90 with OsHV-1, we quantified OsHV-1 DNA in oysters, used electronic microscopy to observe  
91 cell phenotypes, and studied gene, proteomic and metabolic responses during the disease  
92 outbreak. Our results revealed that a harsh fluctuating environment boosts metabolism,  
93 inflammation, and immunity in oysters, promoting resistance to POMS. It involves some

94 changes in the mitochondrial functioning and results in delayed mortality for intertidal  
95 oysters.

## 96 2. MATERIALS AND METHODS

### 97 2.1 *Experimental design*

98 Specific-pathogen free oyster (SPF) spat were produced at Ifremer's laboratory (France;  
99 (Petton et al., 2015) and maintained in a hatchery. They were deployed on the 2<sup>nd</sup> of March  
100 2018 in an experimental site with oyster farming in the Bay of Brest (Brittany, France, 48° 20'  
101 06.19" N, 4° 19' 06.37" W) that belongs to the oyster observatory network ECOSCOPA  
102 (Fleury et al., 2021). The 6 months-old SPF (mean size of ~1.2 cm; mean weight of ~1.5 g)  
103 were placed in regular-sized mesh oyster bags (length: 1 m; width: 0,3 m; mesh: 9 mm  
104 diameter) and the density was 300 oysters per bag (total biomass = 450 g per bag) according  
105 to standard rearing procedures (Fleury et al., 2020). The bags were deployed at three  
106 bathymetric levels (3 bags per bathymetry; 9 bags in total) in the natural limits of wild *C.*  
107 *gigas* repartition in the field: Low =1.6 m above Chart Datum (+CD; subtidal); Middle =3 m  
108 +CD (intertidal); High =5 m +CD (intertidal). Oysters were sampled on 14<sup>th</sup> May 2018. They  
109 were counted and weighed every 15 days until the end of the experiment (13<sup>th</sup> of July) to  
110 monitor growth and mortality, according to the protocol described by the RESCO network  
111 (Mazaleyrat et al., 2022).

### 112 2.2 *In situ* temperature and pressure data monitoring

113 Autonomous data loggers (SP2T© from NKE, Hennebont, France) were used to monitor  
114 temperature and pressure for oysters at each studied bathymetry (one logger per level) with a  
115 record of one data per minute. Immersion time relative to the total submerged tracking time  
116 was calculated with pressure data. The maximum permissible deviation allowed for  
117 temperature data was  $\pm 0.1^{\circ}\text{C}$ . We calculated the time spent  $\geq 16^{\circ}\text{C}$  in seawater,  $\geq 24^{\circ}\text{C}$ , and  
118  $\geq 29^{\circ}\text{C}$  in air, using the number of days multiplied by the temperature of  $16^{\circ}\text{C}$ ,  $24^{\circ}\text{C}$ , or  $29^{\circ}\text{C}$   
119 (expressed in  $^{\circ}\text{C}\cdot\text{day}$ ). Datasets of *in situ* temperature and pressure are available at DOI:  
120 10.17882/79095 (Petton et al., 2020).

### 121 2.3 Sample preparation

122 On 14<sup>th</sup> May 2018, 25 oysters per bag were sampled (25 oysters x 3 bags x 3 bathymetric  
123 levels; 9 bags in total). In each bag, 10 oysters were sampled for OsHV-1 DNA quantification  
124 (n=10 biological samples per bag) and among them, 5 were used for gene expression (n=5  
125 biological samples per bag) and 5 samples were pooled for biochemical analyses, proteomics  
126 and LC-HRMS metabolomics (n= 1 pool of 5 individuals per bag). In addition, 10 oysters  
127 were sampled in each bag for extraction of the mitochondrial-enriched fraction before nano-

128 LC MS/MS proteomic analysis (n= 1 pool of 10 individuals per bag). Then, 5 oysters were  
129 sampled in each bag to dissect the heart for transmission electron microscopy (TEM). All the  
130 analyses were done in triplicates (n= 3 technical replicates).

#### 131 2.4 OsHV-1 DNA quantification

132 Oyster's flesh (n=10 individuals per bag x 3 bags x 3 bathymetric levels) was frozen in liquid  
133 nitrogen after removing the shells, then grounded using an MM400 homogenizer (Retsch,  
134 Eragny, France). OsHV-1 DNA quantification was conducted by LABOCEA (Brest, France)  
135 on total DNA (n=10) extracted with a QIAamp tissue mini kit (Qiagen, Hilden, Germany)  
136 according to (Pepin et al., 2008). The extract was stored at -20 °C before detection and  
137 quantification according to a real-time PCR protocol based on SYBR Green chemistry with  
138 specific primers (Webb et al., 2007). Results were expressed as the log (OsHV-1 DNA copy)  
139 per mg of total DNA.

#### 140 2.5 Transmission electronic microscopy (TEM)

141 The heart, one of the tissues targeted by OsHV-1 (Segarra et al., 2014), was sampled from  
142 live oysters (n=10 per bag) and fixed for 2 h in glutaraldehyde 2.5% diluted in cacodylate  
143 buffer 0.1M pH 7.4. The remaining oyster flesh was kept for further quantification of OsHV-1  
144 DNA (data not shown). The obtained values of OsHV-1 DNA were used to assign the  
145 infection status of the oyster to TEM pictures. Hearts were rinsed in 0.1 M cacodylate buffer  
146 and post-fixed for 2 h in a solution of 1% osmium tetroxide, 1% potassium ferrocyanide in 0.1  
147 M cacodylate buffer to enhance the staining of membranes, rinsed in distilled water,  
148 dehydrated in acetone, then embedded in epoxy resin using an automat Leica EM AMW.  
149 Contrasted ultrathin sections (70 nm) were analyzed under a JEOL 1400 transmission electron  
150 microscope mounted with a Morada CCD camera (Olympus, Rungis, France).

#### 151 2.6 Gene expression analysis

152 Powder of oysters among those used for OsHV-1 DNA (5 individuals per bag x 3 bags x 3  
153 bathymetric levels; 30 mg each) was used for total RNA isolation using 1.5 mL of Extract-all  
154 (Eurobio, Courtaboeuf, France) and extracted with phenol-chloroform according to the  
155 manufacturer's instructions. RNA pellets diluted in molecular biology quality water were  
156 treated with DNase (DNase Max™ Kit; Thermo Fisher Scientific, Les Ulis, France) using 1  
157 U.  $\mu\text{g}^{-1}$  total RNA to remove genomic DNA. Quality and quantity of RNA were determined  
158 using a NanoDrop 2000 (Thermo Fisher Scientific, Les Ulis, France) and a Bioanalyser 2100  
159 (Agilent; Santa Clara, CA, USA) with RNA nano chips (Sussarellu et al., 2016). To verify the  
160 absence of DNA carryover, RNA samples were 1:10 diluted and analyzed in real-time PCR  
161 using elongation factor 1 primers (**Table 1**). First-strand cDNA synthesis was performed

162 using the iScript™ cDNA Synthesis Kit (Bio-rad; Marnes-la coquette, France) with 1 µg  
 163 RNA. We analyzed the relative expression of four genes (**Table 1**): inhibitor of apoptosis *IAP*  
 164 (regulation of cell survival and cell-death processes), an inhibitor of kappa Beta 2 *IKB2*  
 165 (propagation of the cellular response to inflammation), protein kinase RNA-activated *PKR* (a  
 166 potent mediator of antiviral effects exerted by interferons) and Cavortin *CAV* (*or EcSOD*, an  
 167 Extracellular Superoxide Dismutase involved in antioxidant response). Real-time PCR was  
 168 performed in triplicate with 5 µL cDNA (1/20) in 15 µL with final concentrations of 0.2 µM  
 169 each primer, and 1 X SSo Advanced Universal SYBR Green Supermix (Bio-rad; Marnes-la  
 170 coquette, France). Cycling conditions were: activation at 95 °C for 5 min followed by 40  
 171 cycles of 10 sec at 95 °C, 20 sec at 60 °C, and a melting curve program from 69 to 95 °C by  
 172 increasing the temperature by 0.5 °C every 10 sec. Each run included a pool of cDNA as a  
 173 positive control (used as calibrator) and blank controls (water) for each primer pair. PCR  
 174 efficiency ( $E = 10^{(-1/\text{slope})}$ ) was determined by drawing standard curves from a serial dilution  
 175 of the calibrator to ensure that E ranged from 90% to 110% for each primer pair. The relative  
 176 mRNA levels were calculated based on a comparative Ct method (Livak and Schmittgen,  
 177 2001). No difference between Ct values was observed for the gene *MnSOD*. Therefore, the  
 178 relative quantification values of samples were normalized with *MnSOD* level and relative to  
 179 the calibrator, and were expressed in arbitrary units as  $2^{-\Delta\Delta Cq}$  with  $\Delta Cq = Cq$  (studied gene)  
 180  $- Cq$  (*MnSOD*) and  $\Delta\Delta Cq = \Delta Cq$  of cDNA sample  $- \Delta Cq$  of the cDNA calibrator.

181 **Table 1.** Sequences and characteristics of primers used for real-time PCR analyses. Forward  
 182 (F) or reverse (R) primer, nucleotide sequence, product size of the amplicon (bp), and  
 183 efficiency of the primer pair (E). The original publication of each EST/mRNA is given.

184  
 185

Gene name	Ensembl gene ID / Genbank #	ID	F/R	Sequence 5'- 3'	Product size	E (%)	Reference
Inhibitor of apoptosis	XM_034479730	IAP	F R	CCCGAAAACGTAACCTCAGA TTTCGTTTGCTGCTCATTTG	287	99.3	Segarra et al 2014
NF-kappa-B Inhibitor 2	AM856743	IKB2	F R	CAGCATTCACTGACGACGAT TCTGCCTCAGTTTGTGCGTTG	165	100.1	Zhang et al 2011
Eukaryotic translation initiation factor 2-alpha kinase	XM_034478602	PKR (EIF2AK)	F R	GTAGCACCAGGAGATGGTTC GAGCATCAGCAAAGTGTGAG	130	99	Namely PKR in Green & Montagnani 2013
Cavortin (Extracellular superoxide dismutase)	CU681762	CAV (EcSOD)	F R	CTTCATGCCAGGCAACCT TGACGTTGAATCCGGTCA	107	101.4	Gonzalez et al 2005

Manganese superoxide dismutase	CU681620	MnSOD	F R	AGTCTGGTGCACATTCTTGT CATGTGCCAATCAAGATCCTC	111	101.4	Park et al 2009
Elongation factor 1	BQ426516	EF1	F R	GATTGCCACACTGCTCACAT AGCATCTCCGTTCTTGATGC	104	100	Fabioux et al 2004

## 186 2.7 LC-HRMS metabolomic analysis

187 Powder of oysters among those used for OsHV-1 DNA (5 individuals per bag; 20 mg each)  
188 was pooled (1 pool x 3 bags x 3 bathymetric levels) and extracted in 1.4 ml of MeOH,  
189 vortexed 20 sec, put in an ultrasonic bath for 10 min, and centrifuged 2 min (4000 rpm,  
190 20°C). Two different LC-HRMS approaches were applied in this study, namely Reverse  
191 Phase-Metabolomics (RP-metabolomics) targeting semi-polar metabolites, and HILIC Phase-  
192 Metabolomics (HILIC-Metabolomics) for polar metabolites (Cesbron et al., 2017). For RP-  
193 metabolomics, 300 µl supernatant was dried under nitrogen and reconstituted in 50 µl  
194 Water/MeCN (5/95). Chromatographic separation was performed on the Hypersil GOLD C18  
195 column (1.9 µm particle size, 100 x 2.1 mm) and was achieved using a mobile phase of (A)  
196 water/acetonitrile (95/5 w/v) and (B) acetonitrile/water (95/5) each containing 0.1% acetic  
197 acid. The gradient elution was 0-2.40 min, 25% B; 2.40-4.50 min, 70% B; 4.50-11 min, 100%  
198 B with a hold for 3 min; 14-16.5 min, linear decrease to 5% B then hold for 3.5 min. All  
199 sample fingerprinting was performed on a Thermo Ultimate3000 HPLC system coupled to a  
200 Finnigan hybrid mass spectrometer (QExactive, Thermo Fisher Scientific, Les Ulis, France).  
201 The column temperature was set at 35°C with an LC flow of 0.4 mL/min, the vial rack  
202 temperature at 10°C, and the injection volume was 5 µL. Then, a heated electrospray  
203 ionization source (H-ESI) was used in polarity switch mode with the voltage set to -3.00 kV  
204 in negative mode and 3.00 kV in positive mode. The capillary voltage was set to 30 V and the  
205 tube lens offset to 100 V. The sheath and auxiliary gas flows were set to 55 and 6 arbitrary  
206 units, respectively, and the drying gas temperature was set to 350 °C. Mass spectra were  
207 recorded from m/z 65.0 to m/z 975.0 at a resolving power of 35000 Full-Width Half  
208 Maximum (FWHM) measured at m/z 200. The Automatic Gain Control (AGC target) was set  
209 at a high dynamic range ( $5 \times 10^5$ ) with a 100 ms maximum injection time. MS instrument  
210 external calibrations were performed using the Calmix-positive and Calmix-negative standard  
211 solutions for the positive and the negative ionization modes, respectively. For HILIC-  
212 metabolomics, 590 µl were dried under nitrogen and reconstituted in 100 µl of 90/10  
213 acetonitrile/Water. Chromatographic separation was performed on a SeQuant ZIC-HILIC 5  
214 µm, 200 Å 150 x 2.1 mm (Merck KGaA, Gernsheim, Germany) and achieved using a mobile  
215 phase of (A) 10 mM ammonium acetate (pH 4.75) in water and (B) acetonitrile containing 10  
216 mM Ammonium acetate and 1% water (pH 4.75). The used elution gradient (A:B, v/v) was as



217 follows: 5:95 from 0 to 2 min; 20:80 at 5 min; 40:60 at 12 min; 60:40 at 14 min to 16 min;  
218 5:95 at 18 to 28 min. A pooled quality control (QC) sample was prepared to ensure that no or  
219 minimal metabolic information was lost and for system equilibration. QC samples were  
220 extracted along with each sample batch and analyzed throughout the analytical run, to provide  
221 robust quality assurance. Every injection vial was spiked with 1ng/μl of internal standards (L-  
222 Leucine-5,5,5-d3, L-Tryptophan-2,3,3-d3, Indole-2,4,5,6,7-d5-3-acetic acid and 1,14-  
223 Tetradecanedioic-d24 acid). Acquisitions were made on a Thermo Ultimate3000 HPLC  
224 system coupled to a Finnigan hybrid mass spectrometer (QExactive, Thermo Fisher  
225 Scientific, Les Ulis, France). MSCAL6 ProteoMass LTQ/FT-Hybrid, MS instrument  
226 calibration standard mixtures, were obtained from Sigma-Aldrich (Saint Quentin Fallavier,  
227 France). LC-MS metabolomics data (LC-MS negative mode data for itaconate) are available  
228 at <https://www.ebi.ac.uk/metabolights/MTBLS2475>.

## 229 2.8 Nano-LC MS/MS proteomic analysis of mitochondrial-enriched fraction

230 **The flesh of ten individuals per bag (10 individuals x 3 bags x 3 bathymetric levels)** was used  
231 for isolation of mitochondrial-enriched protein extract adapted from (Wang et al., 2016). The  
232 flesh of 10 oysters was dried by dabbing on a paper tissue, weighed, and rinsed on 80 μm  
233 mesh with 1 ml isolation buffer containing 300 mM sucrose, 5 mM TES, 200 mM EGTA,  
234 with antiproteases added extemporaneously (Complete™ Protease Inhibitor Cocktail, Sigma-  
235 Aldrich; Saint Quentin Fallavier, France), pH 7.2. The flesh was then chopped with scissors  
236 and homogenized in the ice-cold isolation buffer at a 1/3 mass volume ratio first slightly in a  
237 motorized Potter tissue grinder (Heidolph, 153 Kelheim, Germany), then by 10 passes in a  
238 Dounce homogenizer. Homogenate was filtered on 80 μm mesh and centrifuged at 900 g at  
239 4°C for 10 min to remove cellular debris. The supernatant was collected, filtered again on 80  
240 μm mesh, and centrifuged at 9,000 g at 4°C for 10 min. The mitochondrial pellet was re-  
241 suspended in 400 μl of ice-cold protein extraction buffer containing 50 mM Bis-Tris, 750 mM  
242 aminocaproic acid, 1% (m/v) n-dodecyl-β-D-maltopyranoside, with antiproteases added  
243 extemporaneously (Complete™ Protease Inhibitor Cocktail, Sigma-Aldrich; Saint Quentin  
244 Fallavier, France), pH 7. Proteins were solubilized overnight at 4°C using a rotary stirrer, then  
245 extracted by centrifugation at 10,000 g for 45 min at 4°C. Protein extracts were homogenized  
246 in concentration then reduced (50 mM DTT) and alkylated (55 mM Iodoacetamide) before  
247 overnight trypsin digestion at 37°C. For nano-LC fragmentation, protein or peptide samples  
248 were desalted and concentrated onto a μC18 Omix (Agilent; Santa Clara, CA, USA). The  
249 chromatography step was performed on a NanoElute (Bruker Daltonics; Bremen, Germany)  
250 ultra-high pressure nanoflow chromatography system. Peptide samples were concentrated

251 onto a C18 pepmap 100 (5 mm x 300  $\mu$ m i.d.) precolumn (Thermo Fisher Scientific, Les Ulis,  
252 France) and separated at 50°C onto a reversed-phase Reprosil column (25 cm x 75  $\mu$ m i.d.)  
253 packed with 1.6  $\mu$ m C18 coated porous silica beads (Ionopticks; Fitzroy, Australia). Mobile  
254 phases consisted of 0.1% formic acid, 99.9% water (v/v) (A) and 0.1% formic acid in 99.9%  
255 acetonitrile (v/v) (B). The nanoflow rate was set at 400 nl/min, and the gradient profile was: 2  
256 to 15% B (60 min), increase to 25% B (30 min), 37% B (10 min), washing step at 95% B, re-  
257 equilibration. MS experiments were carried out on a TIMS-TOF pro mass spectrometer  
258 (Bruker Daltonics; Bremen, Germany) with a modified nanoelectrospray ion source  
259 (CaptiveSpray, Bruker Daltonics; Bremen, Germany). The system was calibrated each week  
260 and mass precision was better than 1 ppm. A 1400 spray voltage with a capillary temperature  
261 of 180°C was typically employed for ionizing. MS spectra were acquired in the positive mode  
262 in the mass range from 100 to 1700 m/z. The mass spectrometer was operated in PASEF  
263 mode with the exclusion of single charged peptides and 10 PASEF MS/MS scans were  
264 performed during 1.25 sec from charge range 2-5. The fragmentation pattern was used to  
265 determine the sequence of the peptide. Database searching was performed using the Peaks X  
266 software. A Uniprot *Crassostrea gigas* database was used. The variable modifications  
267 allowed were as follows: C-Carbamidomethylation, K-acetylation, and methionine oxidation.  
268 "Trypsin" was selected as semispecific. Mass accuracy was set to 30 ppm and 0.05 Da for MS  
269 and MS/MS modes respectively. Data were filtered according to an FDR of 0.5%, two unique  
270 peptides, and protein redundancy elimination based on proteins being evidenced by the same  
271 set or a subset of peptides. To quantify the relative protein abundance levels between groups,  
272 three technical replications of each sample (nine LC-MS/MS runs) were analyzed using the  
273 label-free quantification feature of PEAKS X+ software. Feature detection was separately  
274 performed on each sample by the expectation-maximization-based algorithm. The features of  
275 the same peptide from all samples were aligned through the retention time alignment  
276 algorithms. Mass error tolerance was set at 30 ppm and retention time tolerance at 10 min.  
277 Samples normalization factors were obtained by the total ion current (TIC) of each sample/the  
278 TIC of the reference sample which was automatically chosen by PEAKS. Protein abundance  
279 was calculated using the sum area of the top three unique peptides. Technical repeats of each  
280 sample were merged to give a protein detection profile. The protein abundance levels were  
281 separately compared for biological replicates. A 1.5-fold increase in relative abundance and a  
282 significance  $\geq 10$  using ANOVA were used to determine enriched proteins. In addition,  
283 quality was set  $>2$ , peptides must be detected in the least 2 samples per group and modified  
284 forms were excluded. The mass spectrometry proteomics data have been deposited to the

285 ProteomeXchange Consortium via the PRIDE (Perez-Riverol et al., 2019) partner repository  
286 with the dataset identifier PXD025533.

## 287 2.9 Statistical analyses

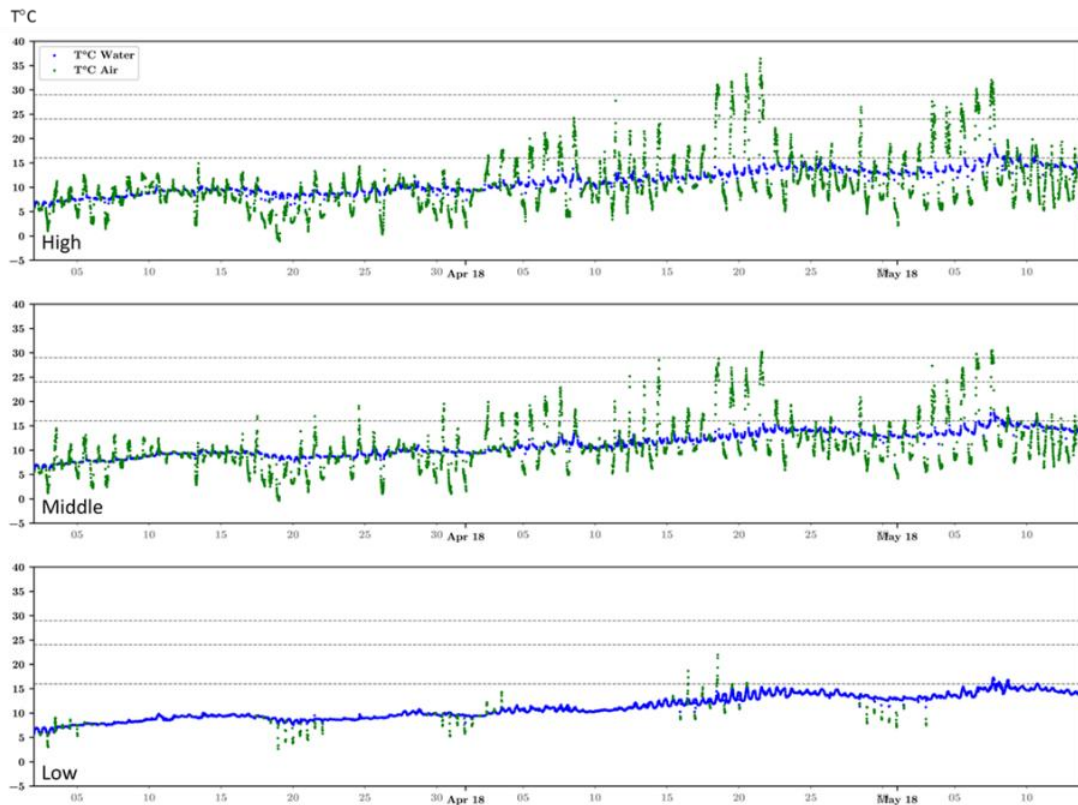
288 The survival curves of oysters were compared among bathymetry using the Cox regression  
289 model. The proportionality of hazards (PH) was checked with martingale residuals (LIN et al.,  
290 1993). Because the PH assumption was violated, time-dependent covariates representing the  
291 interaction of the bathymetry and log time were added to the model. Analyses were conducted  
292 using the SAS software package (SAS 9.4, SAS Institute). Kruskal-Wallis test was conducted  
293 to determine differences in OsHV-1 DNA in oyster tissues at each bathymetry. For other  
294 analyses, the normal distribution of data was checked by the Shapiro test, and the  
295 homogeneity of variances was evaluated using Bartlett's test. One-way ANOVA was done for  
296 gene expression data and targeted metabolomics and Tukey's HSD was used as a post hoc test  
297 to analyze relative gene expression and metabolomics according to the bathymetry. When  
298 necessary, data were log-transformed.

## 299 3. RESULTS

### 300 3.1 Environmental and oyster parameters

301 We analyzed the environmental conditions supported by oysters in the field until the onset of  
302 first mortalities in subtidal oysters at Low bathymetry on the 14<sup>th</sup> of May (**Fig. 1**). Subtidal  
303 oysters at Low bathymetry (1.6 m) presented 3.9% time of air exposure while intertidal  
304 oysters at the Middle (3 m) and High (5 m) bathymetry presented 42.8% or 55.1% time of air  
305 exposure, respectively (**Table 2**). High-frequency data indicated that the seawater temperature  
306 reached 16°C on the 4<sup>th</sup> of May (Low, Middle) and the 21<sup>st</sup> of April (High). Sixteen degrees  
307 corresponds to the minimal seawater temperature required for optimal disease spread and  
308 subsequent mortalities in the field (Pernet et al., 2018). Intertidal oysters at Middle and High  
309 reached aerial temperatures above 24°C and 29°C before the 14<sup>th</sup> of May, the date of  
310 sampling (**Table 2**). And oysters at High, the upper limit of *C. gigas* natural repartition, faced  
311 extreme aerial temperatures ranging from -1.1°C to 36.4°C during emersion. The mortality  
312 rates achieved by oysters on the 14<sup>th</sup> of May at the different bathymetry was 31.2% at Low in  
313 contrast to 0% at Middle and High in intertidal oysters.

314 **Figure 1. Temperature profiles as a function of bathymetry.** Temperature (°C) profiles  
315 until the sampling date (14<sup>th</sup> of May 2018) were obtained for oysters at Low (1,6m) Middle (3  
316 m) and High (5m) bathymetric levels by using autonomous sensors (NKE ©) attached inside  
317 oyster bags. Data was tagged in blue during immersion (T°C Water) and green during  
318 emersion (T°C Air).



319

320 **Table 2.** Environmental characteristics experienced from the 2<sup>nd</sup> of March to the 14<sup>th</sup> of May  
 321 (sampling date) by oysters at Low (1,6 m), Middle (3 m), and High (5 m) bathymetry:  
 322 emersion and immersion duration (% time), temperature (°C min; °C max), time passed above  
 323 16°C, 24°C and 29°C (expressed as °C.day). Data sets are available at DOI: 10.17882/79095.  
 324 Cumulative mortality of oysters at the sampling date is indicated (%).

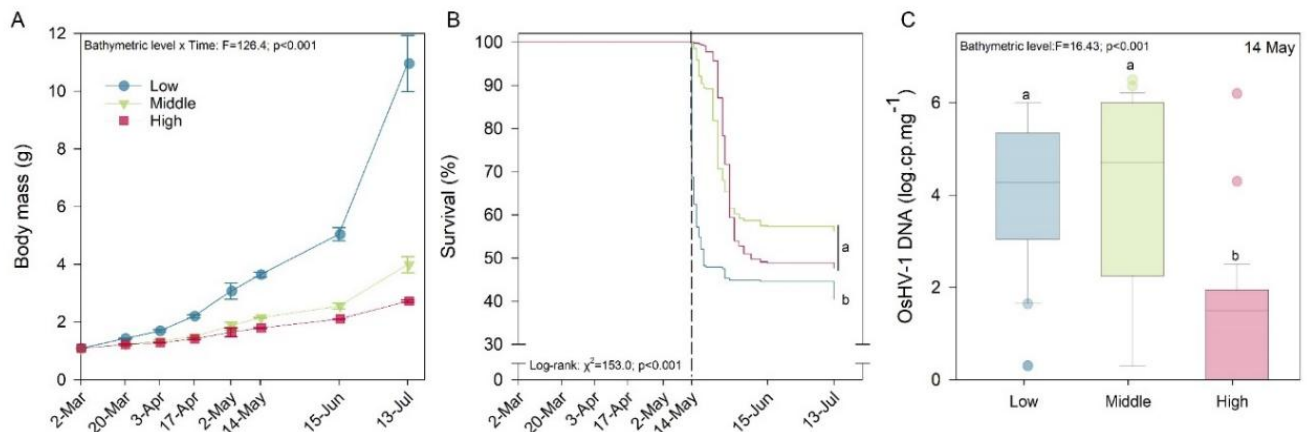
	Emersion			Immersion			°C.day ≥16°C (water)	°C.day ≥24°C (air)	°C.day ≥29°C (air)	Mortality on 14 <sup>th</sup> May (%)
	duration (%)	°C min	°C max	duration (%)	°C min	°C max				
High (5 m)	55.1	-1.1	36.4	44.9	5.9	18.1	0.25	7.69	1.42	0
Middle (3 m)	42.8	-0.4	30.4	57.2	5.9	17.7	0.26	3.23	0.11	0
Low (1.6 m)	3.9	2.6	21.9	96.1	5.7	17.2	0.25	0	0	31.2

### 325 3.2 Energetic reserves, growth, survival, and OsHV-1 DNA amount

326 Intertidal oysters at Middle and High bathymetry lowered their growth as compared to  
 327 subtidal oysters at Low (**Fig. 2A**). The relative amount of energetic reserves (Carbohydrates,  
 328 triacylglycerol/sterol and total protein) was similar in oysters at Low, Middle and High  
 329 bathymetry (**Appendix Table A.1**). Mortalities occurred ten days earlier in subtidal oysters at  
 330 Low compared to intertidal ones at Middle and High bathymetry (**Fig. 2B**). At the onset of  
 331 mortalities, on the 14<sup>th</sup> May, all animals were infected: the level of OsHV-1 DNA was above  
 332 10<sup>5</sup> copy per mg at Low and Middle bathymetry, but below 10<sup>2</sup> copy per mg in the High  
 333 bathymetry conditions, except in two individuals with ≥10<sup>5</sup> copy per mg (**Fig. 2C**). At the end

334 of our experiment, the final survival rate was lightly but statistically increased in intertidal  
 335 oysters to 57% at Middle and 48% at High bathymetry, as compared to subtidal oysters with  
 336 41% survival rate at Low bathymetry (**Fig. 2B**).

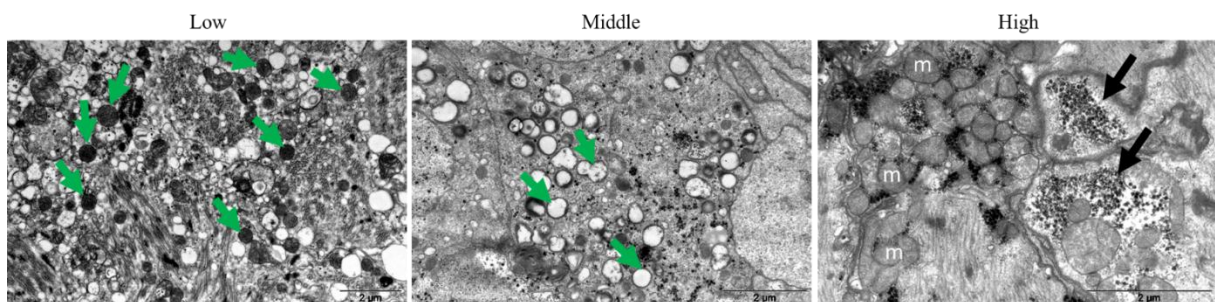
337 **Figure 2. Ecophysiological parameters of oysters.** (A) Body mass (g) and (B) survival (%)  
 338 of oysters (n=300) at Low (1,6 m; blue), Middle (3 m; green) and High (5 m; red) bathymetry.  
 339 (C) Quantification of OsHV-1 DNA on the 14<sup>th</sup> of May; n= 30 individuals per bathymetry;  
 340 data were log (x+1) transformed and expressed as the log (OsHV-1 DNA copy) per mg of  
 341 total DNA.



342  
 343 **3.3 Ultrastructural modifications of heart cells**

344 Transmission electronic microscopy (TEM) evidenced numerous lysosomes in heart cells in  
 345 oysters at Low and Middle bathymetry, suggesting a higher lysosomal activity in oysters that  
 346 presented a high level of OsHV-1 DNA (**Fig. 3**). In contrast, oysters at High bathymetry  
 347 presented clear and rounded mitochondria as well as glycogen stored in rosettes.

348 **Figure 3. Transmission Electronic microscopy analyses.** TEM pictures of cardiomyocytes  
 349 in oysters (n=4 per bathymetry) at Low (1,6 m), Middle (3 m), and High (5 m) bathymetry on  
 350 the 14<sup>th</sup> of May. Green arrows show lysosomes, black arrows show glycogen stocks; (m)  
 351 mitochondria; size is indicated with ladder lower right.

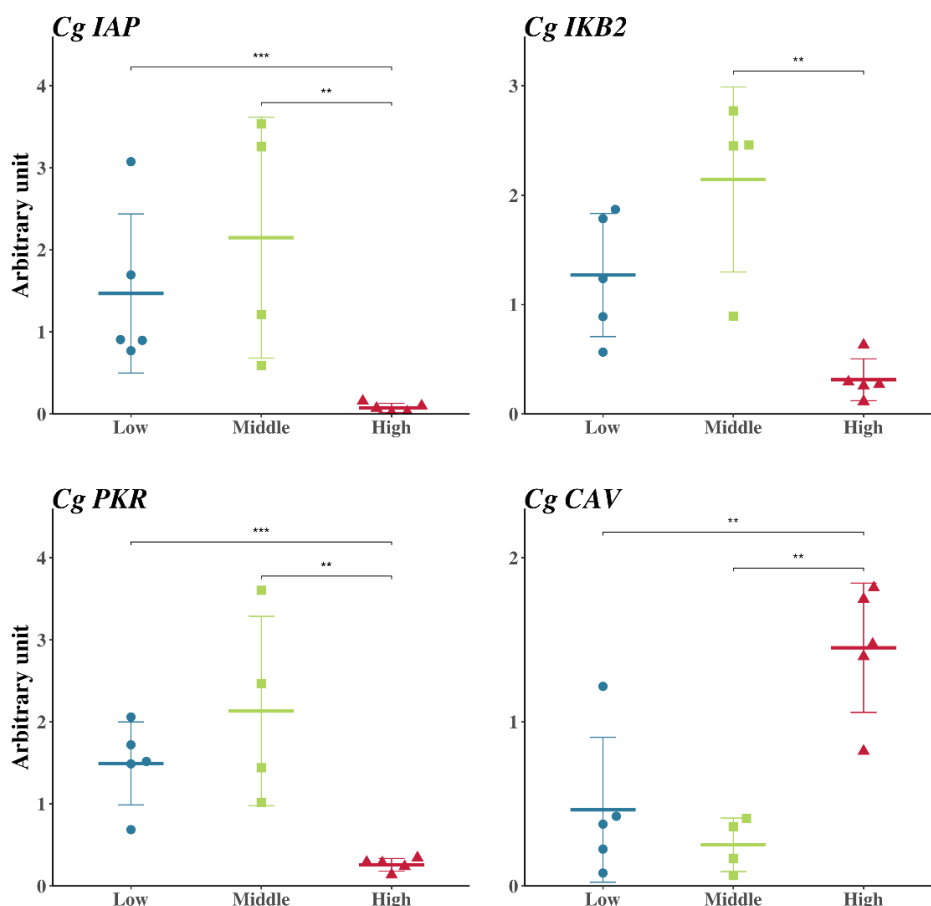


353  
 354

355 3.4 Relative expression of immune-genes *IAP*, *IKB2*, *PKR*, and *CAV*

356 Oysters at Low and Middle bathymetry presented a high amount of *Cg IAP*, *Cg IKB2*, and *Cg*  
357 *PKR* mRNA (**Fig. 4**). These genes are involved in the anti-viral response of *C. gigas* to  
358 OsHV-1 (Pauletto et al., 2017). Our results showed that oysters at High bathymetry presented  
359 an important amount of *Cg CAV* mRNA while they had a low viral load. The cavortin *Cg*  
360 *CAV* encodes for the major protein secreted in response to stress in the hemolymph of *C.*  
361 *gigas* and is involved in defense against bacteria (Green et al., 2014; Itoh et al., 2011; Scotti et  
362 al., 2007). A correlative approach revealed that *Cg CAV* gene expression was negatively  
363 correlated to OsHV-1 DNA quantity (Pearson's  $r = -0.42$ ;  $p$ value = 0.0214; **Table 3**).

364 **Figure 4. Immune gene expression.** Relative expression of *Cg IAP*, *Cg IKB2*, *Cg PKR*, and  
365 *Cg CAV* in oysters ( $n=5$  per level) at Low (1,6 m), Middle (3 m), and High (5 m) bathymetry.  
366 Data are expressed in arbitrary units relative to the *MnSOD* transcript level, as mean  $\pm$  SEM  
367 (\*\* $p < 0.1$ ; \*\*\* $p < 0.01$ ).



368

369



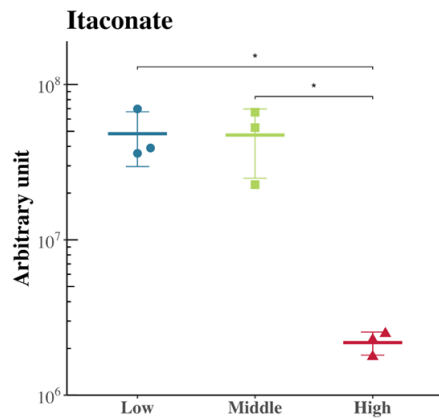
370 **Table 3.** Individual molecular data of *Cg* CAV mRNA (relative expression expressed in  
 371 arbitrary units relative to the *MnSOD* transcript level) and OsHV-1 DNA (copy per mg of  
 372 total DNA) used for the correlative study.

	Bathymetry	<i>Cg</i> CAV mRNA	OsHV-1 DNA
N51	Low	0.42	$2.27 \cdot 10^5$
N52	Low	0.08	$2.26 \cdot 10^5$
N53	Low	0.38	$7.72 \cdot 10^5$
N48B	Low	0.22	$1 \cdot 10^6$
N55B	Low	1.22	$1 \cdot 10^6$
N73B	Middle	1.67	$6.15 \cdot 10^3$
N65	Middle	0.36	$1.71 \cdot 10^6$
N71	Middle	0.06	$1.64 \cdot 10^6$
N72	Middle	0.17	$1.08 \cdot 10^6$
N75	Middle	0.41	$2.30 \cdot 10^6$
N76	High	1.47	$4.94 \cdot 10^1$
N79	High	1.82	$6.06 \cdot 10^1$
N80	High	1.75	$2.66 \cdot 10^1$
N82	High	0.82	$6.12 \cdot 10^1$
N89	High	1.40	$3.21 \cdot 10^1$

373 **3.5 Itaconate relative amount**

374 Metabolomic analyses identified statistical changes in the level of itaconate, an anti-  
 375 inflammatory metabolite produced by immune cells (Rosani et al., 2019), as a function of  
 376 bathymetry. We showed that the itaconate relative amount increased in oysters at Low and  
 377 Middle bathymetry (**Fig. 5**), which presented a high virus load. In contrast, oysters at High  
 378 bathymetry, with a low virus load, presented an itaconate amount decreased by 10 times (**Fig.**  
 379 **5**).

380 **Figure 5. Metabolic analysis of Itaconate relative amount.** Relative quantification of the  
 381 metabolite itaconate in oysters (n=3 per level) at Low (1,6 m), Middle (3 m), and High (5 m)  
 382 bathymetry. Data are calculated as the area under the curve and expressed in arbitrary units as  
 383 mean  $\pm$  SE (\*p<0.05).



384

385

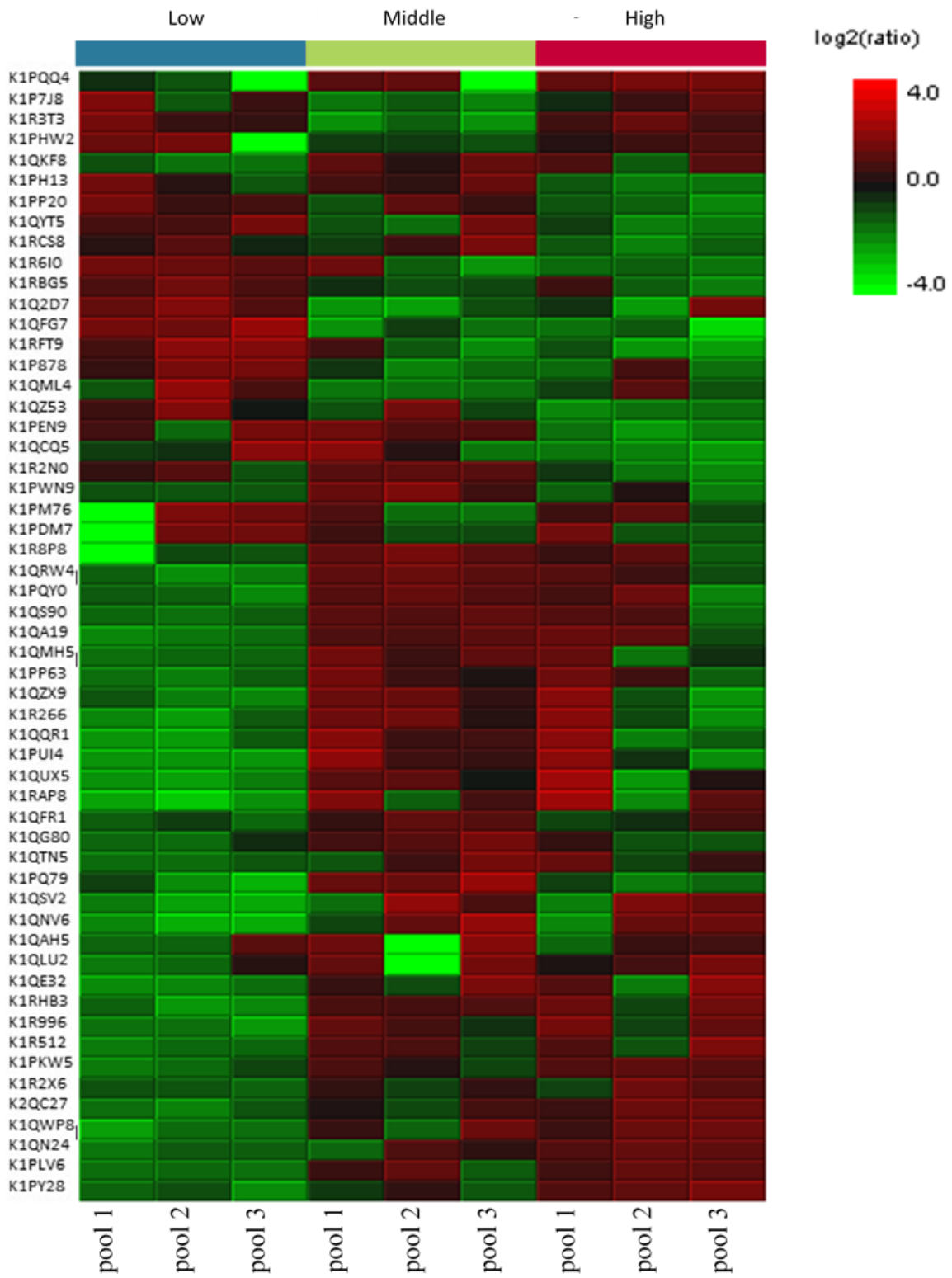
### 386 3.6 Proteomic changes in intertidal oysters

387 Proteomic analyses identified 55 proteins differentially expressed in oysters as a function of  
 388 the Middle and High bathymetry compared to Low bathymetry ( $p \leq 0.05$ ; **Fig. 6**). **Table 4**  
 389 shows the list of identified proteins and the functional properties associated, based on the  
 390 Uniprot database (<http://www.uniprot.org/>). The proteins differentially expressed were  
 391 mitochondrial, transmembrane, and cytoplasmic, among them, 10 proteins still had an  
 392 unknown function.

393 **Figure 6. Proteomic analysis.** Heatmap representing significantly differentially expressed  
 394 proteins (55 in total) in the mitochondrial-enriched protein fraction of oysters (pools of  $n= 10$   
 395 individuals) at Low (1,6 m), Middle (3 m), and High (5 m) bathymetry. Enrichment intensity  
 396 is expressed as the ratio between proteins up-regulated (red heat) and down-regulated (green  
 397 heat) normalized with the total.

398





399  
400  
401

402 **Table 4.** Identification of proteins down-expressed (bold in grey) or over-expressed at Middle  
403 and High compared to Low bathymetry (significance  $\geq 10$  using ANOVA). The abundance of  
404 proteins was expressed as a ratio by comparison with Low (ratio = 1).

Uniprot accession	NCBI accession	Protein name	Significance	Ratio			Biological process
				Low	Middle	High	
K1PQQ4	CGI 10008275	L-rhamnonate dehydratase	11.34	1	1.48	1.72	Carbohydrate metabolism
K1P7J8	CGI 10008151	6-phosphofructokinase	11.86	1	0.53	0.94	Glycolysis
K1R3T3	CGI 10019268	Transcription factor BTF3	13.48	1	0.45	0.98	Transcription
K1PHW2	CGI 10012107	<i>Unknown</i>	18.49	1	0.59	0.72	Membrane cell adhesion
K1QKF8	CGI 10022811	S-(hydroxymethyl)glutathione dehydrogenase	14.01	1	1.75	1.50	Detoxification
K1PH13	CGI 10012206	Glycosyltransferase subunit STT3B	14.21	1	1.06	0.61	Protein N-glycosylation
K1PP20	CGI 10013293	Ependymin-related protein 1	10.51	1	0.85	0.56	Cell matrix adhesion
K1QYT5	CGI 10012871	Phosphate carrier protein	10.08	1	0.79	0.55	OXPPOS Mitochondrial carrier
K1RCS8	CGI 10013133	Metalloendopeptidase	10.12	1	1.11	0.64	Mitochondria quality control
K1R610	CGI 10017526	<i>Unknown</i>	22.41	1	0.64	0.49	<i>Unknown</i>
K1RBG5	CGI 10021542	4-hydroxybutyrate coenzyme A transferase	10.57	1	0.70	0.63	Detoxification
K1Q2D7	CGI 10004665	Putative ubiquitin carboxyl-terminal hydrolase FAF-X	10.92	1	0.37	0.66	Protein deubiquitination
K1QFG7	CGI 10005276	Galactocerebrosidase	13.48	1	0.46	0.37	Glycolipids catabolism
K1RFT9	CGI 10023709	L-rhamnose-binding lectin	12.56	1	0.49	0.34	Innate immunity
K1P878	CGI 10007259	Universal stress protein	10.8	1	0.51	0.57	Resistance to stress
K1QML4	CGI 10018739	<i>Unknown</i>	10.48	1	0.46	0.72	AA catabolism
K1QZ53	CGI 10013854	<i>Unknown</i>	12.11	1	0.84	0.47	<i>Unknown</i>
K1PEN9	CGI 10001281	Endoglucanase	16.76	1	1.14	0.48	Carbohydrate metabolism
K1QCQ5	CGI 10016417	Succinate-CoA ligase subunit $\beta$	10.12	1	0.92	0.41	KREBS cycle
K1R2N0	CGI 10008056	Histone H4	10.12	1	1.22	0.67	Transcription initiation
K1PWN9	CGI_10010245	Mannose receptor 1	10.42	1	1.71	0.96	Membrane receptor (pathogen)
K1PM76	CGI_10020978	NADH dehydrogenase 1 $\alpha$ subunit 9	11.73	1	0.52	0.68	OXPPOS complex I
K1PDM7	CGI_10008106	Multidrug resistance-associated protein 1	14.96	1	0.62	0.70	Resistance to stress
K1R8P8	CGI_10024629	Neprilysin	16.18	1	1.65	1.23	Inflammation
K1QRW4	CGI_10025126	Coronin	15.92	1	2.2	1.59	Cytoskeleton dynamic
K1PQY0	CGI_10010860	<i>Unknown</i>	12.07	1	1.90	1.56	<i>Unknown</i>
K1QS90	CGI_10002881	Neuroglian	25.26	1	1.79	1.45	Cell adhesion
K1QA19	CGI_10015782	Calmodulin-like protein 3	19.18	1	2.01	1.98	Resistance to stress
K1QMH5	CGI_10018703	Small nuclear ribonucleoprotein Sm D1	14.98	1	1.88	1.42	Splicing
K1PP63	CGI_10005728	Carboxylic ester hydrolase	11.89	1	1.83	1.67	Detoxification
K1QZX9	CGI_10014226	<i>Unknown</i>	12.81	1	2.01	1.74	<i>Unknown</i>
K1R266	CGI_10026868	Retinal dehydrogenase 1	11.06	1	2.38	1.93	Detoxification
K1QQR1	CGI_10024475	Major vault protein	10.46	1	2.58	2.00	Innate immunity
K1PUI4	CGI_10005346	Peptidylprolyl isomerase	13.38	1	3.27	3.04	Chaperone
K1QUX5	CGI_10021866	Omega-crystallin	17.85	1	2.55	2.91	Detoxification
K1RAP8	CGI_10002873	Malic enzyme	11.87	1	3.30	3.88	Lipid metabolism

K1QFR1	CGI_10013834	Beta-1,3-glucan-binding protein	13	1	1.53	1.26	Innate immunity
K1QG80	CGI_10018743	Unknown	11.36	1	1.66	1.14	Unknown
K1QTN5	CGI_10010936	Collagen alpha-1(XIV) chain	10	1	1.69	1.38	Cell adhesion
K1PQ79	CGI_10011897	Copine-3 ser thr kinase	13.4	1	3.08	1.33	Cell adhesion
K1QVS2	CGI_10009327	Thioredoxin domain-containing protein 5	10.2	1	3.17	2.91	Chaperone
K1QNV6	CGI_10013164	Tropomyosin	13.97	1	3.98	2.99	Cytoskeleton dynamic
K1QAH5	CGI_10012180	Integrin beta	10.57	1	1.86	1.06	Cell adhesion
K1QLU2	CGI_10017638	Serine protease inhibitor dipetalogastin	11.12	1	1.90	1.61	Inflammation
K1QE32	CGI_10018790	Acyl-CoA dehydrogenase	10.67	1	2.16	2.23	Lipid metabolism
K1RHB3	CGI_10022015	Phosphoenolpyruvate phosphomutase	11.61	1	2.08	2.32	Reservoir of organic phosphorus
K1R996	CGI_10001478	Long-chain-fatty-acid-CoA ligase 4	13.47	1	2.01	2.24	Lipid metabolism
K1R512	CGI_10026535	Unknown	14.63	1	1.53	1.75	Unknown
K1PKW5	CGI_10008456	Unknown	13.66	1	1.41	1.72	Unknown
K1R2X6	CGI_10018375	Unknown	12.75	1	1.26	1.53	Unknown
K1QC27	CGI_10023479	Hydroxysteroid dehydrogenase-like protein 2	14.12	1	1.49	1.98	Lipid metabolism
K1QWP8	CGI_10022729	Actin-2	11.99	1	1.89	2.32	Cytoskeleton dynamic
K1QN24	CGI_10017980	Carboxypeptidase B	18.5	1	1.36	1.81	Proteolysis
K1PLV6	CGI_10007483	F-actin-capping protein subunit alpha	20.75	1	1.58	1.87	Cytoskeleton dynamic
K1PY28	CGI_10006807	Sarcoplasmic calcium-binding protein	13.62	1	1.35	2.01	Cytoskeleton dynamic

405

### 406 **3.6.1 Metabolic reprogramming in intertidal oysters.**

407 The expression of 16 metabolic proteins was modified in intertidal oysters at Middle and High  
408 bathymetry (27% of proteomic changes), indicating a metabolic reprogramming in oysters  
409 supporting the fluctuating environment despite we were not able to detect any modifications  
410 in total energy reserves in the whole body (Appendix Table A.1). The L-rhamnonate  
411 dehydratase (K1PQQ4), implicated in fructose and mannose metabolism, was up-regulated  
412 and the 6-phosphofructokinase (K1P7J8) which catalyzes the phosphorylation of fructose-6-  
413 phosphate to fructose 1,6-bisphosphate during glycolysis, was down-regulated. Protein N-  
414 glycosylation (K1PH13) and protein deubiquitination (K1Q2D7) were down-regulated and  
415 carbohydrate metabolism was also decreased (glycolipids K1QFG7 and cellulose catabolism  
416 K1PEN9). As further evidence of metabolic changes, the detoxification of phase 1 metabolic  
417 products was enhanced (detoxification of ethanol: K1QKF8; xenobiotic: K1PP63; aldehyde:  
418 K1R266, K1QUX5; other: K1RBG5). Proteomic changes also concerned the regulation of  
419 lipid metabolism suggesting an acceleration of the lipid's turn-over (synthesis and oxidation).  
420 Indeed, both the malic enzyme (K1RAP8), which conducts excess ethanol-derived energy  
421 into lipid synthesis, and the mitochondrial long-chain specific Acyl-CoA dehydrogenase

422 (K1QE32), that catalyzes the first step of the fatty-acid beta-oxidation, were up-regulated, as  
423 well as the Long-chain-FA-CoA ligase 4 (K1R996) that catalyzes the conversion of long-  
424 chain FA to their active form acyl-CoA before lipogenesis and lipolysis. The up-regulation of  
425 the hydroxysteroid dehydrogenase (K1QC27) reflected changes in steroid metabolism and an  
426 increased amount of carboxypeptidase B was indicative of changes in the digestive gut of  
427 intertidal oysters (Yang et al., 2020).

### 428 ***3.6.2 Changes in mitochondrial metabolism in intertidal oysters.***

429 Changes in mitochondrial metabolism were reflected by the differential expression of 4  
430 mitochondrial proteins (6% of proteomic changes). The phosphate carrier protein (K1QYT5)  
431 which is located in the mitochondrial inner membrane and catalyzes the transport of  
432 phosphate ions for oxidative phosphorylation OXPHOS, and the NADH dehydrogenase 1 $\alpha$   
433 subunit 9 (K1PM76) which is involved in the mitochondrial respiratory chain (OXPHOS  
434 complex I), were down-regulated. Expression of the mitochondrial metalloendopeptidase  
435 (K1RCS8), involved in the quality control system of the inner membrane of mitochondria  
436 under stress, was decreased in intertidal oysters at High bathymetry. The Succinate-CoA  
437 ligase subunit  $\beta$  (K1QCQ5), a matrix mitochondrial protein that hydrolyses succinyl-CoA for  
438 the synthesis of ATP, was down-regulated, indicating a lower mitochondrial TCA functioning  
439 (KREBS cycle).

### 440 ***3.6.3 Boost of inflammation and immunity in intertidal oysters.***

441 Differential expression of 19 proteins (32% of proteomic changes) concerned inflammation  
442 and immunity. Lectins are critical immune effectors of cellular defense in hemocytes of  
443 marine invertebrates (He et al., 2015; Watanabe et al., 2009) and we showed that two  
444 transmembrane lectin receptors (K1RFT9, K1PWN9) were down-regulated. The changes  
445 observed in the expression of the mannose receptor 1 (K1PWN9), a membrane receptor of  
446 immune cells involved in pathogen recognition (Jia et al., 2021), were indicative of changes  
447 in immunity. Neprilysin (K1R8P8), an invertebrate immunoregulator, was up-regulated and it  
448 is a membrane biomarker of activated hemocytes (Ottaviani et al., 2012). Up-regulation of  
449 major vault protein (K1QQR1) and beta-1,3-glucan-binding protein (K1QFR1) reflected  
450 increased responsiveness of the innate immune system to the internalization of pathogens  
451 (Jenkins, 2008; Melillo et al., 2018; Phupet et al., 2018). The immune Ser-protease inhibitor  
452 (K1QLU2) was up-regulated, reflecting enhanced protection against pathogens or parasites  
453 (Kanost, 1999). Associated with the boost in immunity, our results showed an increase in  
454 cytoskeletal and cell dynamics reflected by the up-regulation of 9 proteins (cell-matrix  
455 adhesion K1PP20; coronin K1QRW4; neuroglian K1QS90; collagen alpha-1 chain K1QTN5;

456 copine 3 ser-thr kinase K1PQ79; tropomyosin K1QNV6; integrin beta K1QAH5; actin-2  
457 K1QWP8; F-actin-capping protein subunit alpha K1PLV6; sarcoplasmic calcium-binding  
458 protein K1PY28), as well as the increase of chaperone activity (Chawsheen et al., 2018)  
459 (Peptidylpropyl isomerase K1PU14; thioredoxin domain-containing protein 5 K1QVS2)  
460 reflecting changes in vesicular transport, cell migration and cell structure in intertidal oysters.  
461 All of these processes are involved in the immune reactions of hemocytes (Rybakin and  
462 Clemen, 2005).

#### 463 **3.6.4 Stress proteins in intertidal oysters.**

464 Differential expression of 6 stress proteins (10% of proteomic changes) was evidenced. The  
465 universal stress protein USP (K1P878) and the Multidrug resistance-associated protein 1, an  
466 ATP-binding mitochondrial transmembrane transporter (K1PDM7), were down-regulated in  
467 intertidal oysters submitted to environmental fluctuations, although both proteins are  
468 expressed under environmental multi-stress in animals, plants and bacteria (Tkaczuk et al.,  
469 2013; Vollmer and Bark, 2018). Calmodulin-like protein 3 (K1QA19), a stress-signal  
470 transducer involved in Ca<sup>2+</sup> signaling pathways activated by environmental stress or  
471 pathogens, was up-regulated. In addition, the down-regulation of the transcription factor  
472 BTF3 from the ARN polymerase II complex (K1R3T3) and up-regulation of the splicing  
473 factor ribonucleoprotein SmD1 (K1QMH5) and histone H4 (K1R2N0) indicated important  
474 changes in the regulation of gene expression in intertidal oysters.

#### 475 **3.6.5 Intertidal oysters at the upper natural limit of bathymetry.**

476 Interestingly, intertidal oysters reared at the upper limit of bathymetry (High) specifically  
477 down-regulated 5 proteins as compared to intertidal oysters at Middle bathymetry. Down-  
478 regulation of the mannose receptor 1 (K1PWN9) was indicative of lowered immune cells'  
479 pathogen recognition (Jia et al., 2021). The mitochondrial metalloendopeptidase (K1RCS8),  
480 which stimulates the mitochondrial quality control mechanisms in response to hypoxia-  
481 reoxygenation stress in *C. gigas* (Sokolov et al., 2019), was down-regulated, reflecting that  
482 the mitochondrial functioning might be more deeply modified at High bathymetry. The  
483 subunit STT3B (K1PH13) was lowered, indicating fewer misfolded proteins in the  
484 endoplasmic reticulum, *i.e.* no ER stress for intertidal oysters at High bathymetry despite their  
485 harsh conditions. Down-regulated endoglucanase (K1PEN9) reflected lowered cellulose  
486 catabolic process and down-regulation of histone H4 (K1R2N0), a core component of the  
487 nucleosome (Keating and El-Osta, 2015; Zacchi et al., 2010), might reflect some chromosome  
488 decondensation at High bathymetry.

## 489 **4. DISCUSSION**

#### 490 4.1 **Host-pathogen interaction is modulated by the bathymetry.**

491 *C. gigas* are exposed to a gradient of environmental stress along subtidal and intertidal  
492 habitats that shapes their phenotype, such as increased tolerance to hypoxia in intertidal  
493 oysters (Meng et al., 2018). Here we showed that intertidal oysters reared at 3.5 and 6 meters  
494 of bathymetry delayed by ten days the onset of the mortality induced by OsHV-1 and  
495 increased their final survival by a maximum of 17%. Previous field experiments showed that  
496 the final survival rate increased by 8% (Pernet et al., 2019) or 15% (Azéma et al., 2017) in  
497 intertidal oysters. Here we showed that intertidal oysters did not modify their energetic  
498 composition (carbohydrates, TAG/sterol, total protein amount), but revealed some proteomic  
499 changes indicative of metabolic reprogramming in response to harsh environmental  
500 conditions. Intertidal oysters at Middle bathymetry remained susceptible to OsHV-1 infection,  
501 indicating that the metabolic reprogramming and the reduced immersion time, generating less  
502 contact time with the virus in seawater, did not block the viral infection. **As a response to the**  
503 **viral attack, oysters at Low and Middle bathymetry over-expressed key immune-responsive**  
504 **genes (*Cg-IAP*, *Cg-IKB2*, and *Cg-PKR*) and increased production of the metabolite itaconate,**  
505 **independently of their habitat.** Itaconate was already characterized as a non-specific  
506 immunological biomarker of pathogens in marine bivalves, such as *C. gigas* oyster larvae  
507 infected by OsHV-1 and *Perna canaliculus* mussels infected by *Vibrio splendidus* (Nguyen et  
508 al., 2019, 2018; Van Nguyen and Alfaro, 2019). **These changes in gene expression combined**  
509 **with itaconate production reflected a strong anti-viral immune response that was similar in**  
510 **subtidal or intertidal oysters that presented a high virus load, despite their differences in**  
511 **environmental conditions. However, such anti-viral response did not predict the oyster**  
512 **susceptibility to death since oysters at Middle remained better protected from mortality. All**  
513 **together, our results indicated that a harsh intertidal environment can influence gene**  
514 **expression and metabolite production in *C. gigas* without altering their ability to activate an**  
515 **anti-viral immune response.**

#### 516 4.2 **Immune-metabolism is modified by bathymetry.**

517 No deep changes in energetic reserves were obtained at the level of the whole body,  
518 consistent with the similar carbohydrates, lipid, and protein amounts detected. In contrast, the  
519 proteomic study highlighted an intertidal metabolic footprint that may confer an advantage to  
520 intertidal oysters facing POMS, through an interaction between environment, metabolism, and  
521 immunity, also called immune-metabolism (Galenza and Foley, 2019). The intertidal oysters  
522 at Middle and High bathymetry reprogrammed their metabolism toward enhanced  
523 neoglucogenesis, increased lipid turn-over, and decreased OXPHOS, with activation of

524 inflammation and innate immunity. These proteomic changes delayed the onset of first  
525 mortalities but did not block OsHV-1 intracellular processes, since intertidal oysters at Middle  
526 bathymetry were infected by OsHV-1. Thanks to our study, we can emphasize that intertidal  
527 oysters delayed the mortality because they might be better protected against bacteria, the  
528 second step of POMS, rather than against the virus, the first step of POMS. Indeed, before our  
529 experiment, we deployed 1-year-old *C. gigas* spat in the field to study the bathymetric  
530 influence on their microbiota (Offret et al., 2020). We proved that the diversity of endogenous  
531 microbiota in the digestive gland of oysters was shaped by intertidal conditions at Middle and  
532 High bathymetry (Offret et al., 2020). In our study, we can suppose that intertidal oysters at  
533 Middle and High bathymetry have modified their interaction with bacteria, among them the  
534 opportunistic bacteria involved in the polymicrobial disease (de Lorgeril et al., 2018).  
535 Interestingly, among proteomic changes in intertidal oysters, we detected an increased amount  
536 of carboxypeptidase B (Yang et al., 2020) suggesting that their digestive gut system might  
537 have been modified. As demonstrated in fish, the gut system is considered an important  
538 component of adaptive immunity and resistance to viral disease (Talwar et al., 2018). As  
539 compared to subtidal oysters, intertidal oysters could thus have shaped their digestive  
540 bacterial microbiota as a result of harsh environmental conditions (Offret et al., 2020), leading  
541 to better protection against fatal bacteremia during POMS (de Lorgeril et al., 2018).  
542 Unfortunately, we were not able to analyze bacterial load and diversity in infected oysters in  
543 our study. Studying the effects of bathymetry on oyster microbiota during POMS is now of  
544 further interest.

#### 545 4.3 Mitochondria is involved in host-pathogen interactions.

546 Oysters at Low and Middle bathymetry presented a high amount of OsHV-1 DNA, activated  
547 an immune antiviral response, increased lysosomal activity, and increased itaconate  
548 production. Itaconate is an anti-inflammatory metabolite that is produced by immune cells in  
549 *C. gigas*, as shown in response to an exacerbated inflammatory response during OsHV-1 or  
550 bacterial infection (Nguyen et al., 2019; Van Nguyen and Alfaro, 2019; Young et al., 2017).  
551 Thus, itaconate might play a role in OsHV-1 intracellular processes during POMS by  
552 targeting the mitochondria. In vertebrates, itaconate regulates innate immunity and  
553 inflammation by targeting the mitochondrial metabolism, by blocking the mitochondrial  
554 succinate dehydrogenase (Domínguez-Andrés et al., 2019; Hooftman and O'Neill, 2019; Liao  
555 et al., 2019; Mills et al., 2018; O'Neill and Artyomov, 2019). It participates in the type I  
556 interferon pathway, a key element of immune cell activation. Under pathogen infection,  
557 itaconate can lead to fatal immune paralysis, as a poison of the mitochondria (O'Neill et al.,

2016). Itaconate could serve the virus to manipulate the mitochondria to its advantage, such as many viruses in vertebrates and invertebrates controlling host cell machineries by inhibition of specific signaling pathways (Chen et al., 2011; Rosani et al., 2019; Sanchez and Lagunoff, 2015; Su et al., 2014; Young et al., 2017), these pathways being conserved in *C. gigas* (Epelboin et al., 2016). Itaconate is a key component of metabolic reprogramming in immune cells in vertebrates, linking cell metabolism and the Warburg effect with oxidative and immune responses (Domínguez-Andrés et al., 2019; Hooftman and O'Neill, 2019; O'Neill and Artyomov, 2019). Further studies should be conducted to study the effect of itaconate on the mitochondrial functioning and cell metabolism in *C. gigas*, in particular its role in the Warburg effect that plays in favor of OsHV-1 (Corporeau et al., 2014).

#### 4.4 Can bathymetry cause environmental fever?

In the field, oysters are permissive to OsHV-1 when immersed in seawater between 16°C to 24°C (Pernet et al., 2012). In experimental conditions, immersion in seawater at 29°C induces profound transcriptomic changes that promote oyster survival to OsHV-1, by up-regulation of immune regulatory, anti-apoptosis, and protein process genes, and down-regulation of catabolism, metabolite transport, and growth genes, reflecting changes in the metabolism under thermal stress that decrease their susceptibility (Delisle et al., 2020, 2018). In our study, we observed that intertidal oysters delayed mortality when they spent several hours above 24°C and 29°C in air temperature. A heat-stress response might have been activated in oysters at Middle and High bathymetry, as detected in our proteomic analyses through the over-expression of two chaperone molecules involved in protein folding (Peptidylprolyl isomerase, Thioredoxin domain-containing protein 5). As ectotherms, *C. gigas* physiology and response to pathogens are controlled by temperature and intertidal oysters could thus benefit from an "environmental fever" during emersion. It could resemble the "behavioral fever" of ectothermic vertebrates, such as zebrafish moving to warmer environments to amplify their innate immunity against viral disease (Boltaña et al., 2013; Jia et al., 2014). Indeed, in plants and invertebrates, the innate immune system is shaped by the environment and lifestyle (diet and microenvironment) (Melillo et al., 2018), the heat-stress amplifying immune training, as demonstrated in shrimp (Jia et al., 2014). Such immune training can even confer an immunological memory, also called immune priming, resulting in a faster and more effective response to stress (Melillo et al., 2018; Netea et al., 2020). We already know that immune priming is possible in *C. gigas* after poly I:C injection that induced an antiviral alert and protected oysters from POMS for 4 months (Lafont et al., 2020). Thus, the intertidal environment could have activated a sort of "environmental priming" of *C. gigas*, involving a



592 thermal stress-response mimicking the “behavioral fever” of mobile species such as fish.  
 593 Further experiments are needed to decipher whether immune cells of intertidal oysters were  
 594 primed transiently or long-term, and if they modified their epigenetic status, as a signal of  
 595 "environmental priming".

## 596 5. CONCLUSION

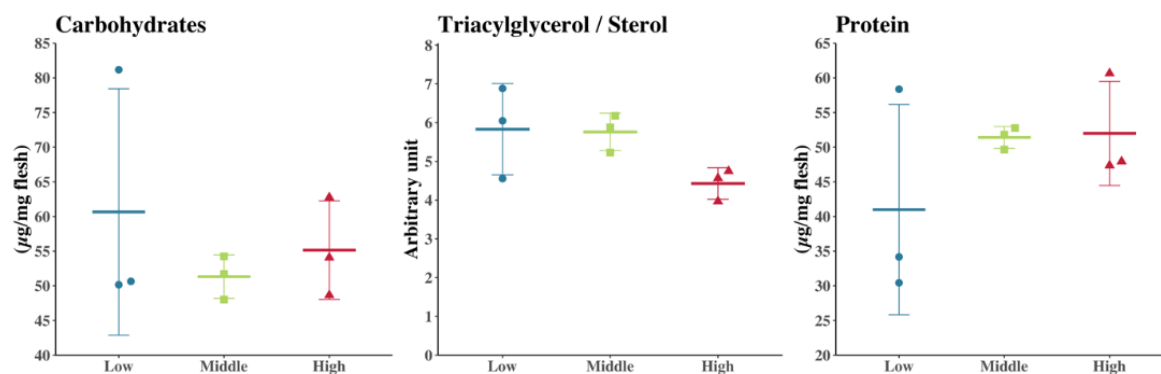
597 Our work demonstrated that fluctuating environmental dynamics influence the plasticity of  
 598 metabolism and immunity in *C. gigas*. The intertidal environment can boost metabolic,  
 599 inflammation, and immune state in juvenile *C. gigas* in a way that modifies interaction with  
 600 pathogens and promotes resistance to POMS. We propose to take advantage of the important  
 601 metabolic plasticity of the Pacific oyster *C. gigas* to adapt to challenging coastal  
 602 environments as a model species to study cellular responses to a harsh environment and the  
 603 impact of global changes on animal health.

## 604 6. APPENDIX

### 605 **Table A.1: Biochemical analyses of carbohydrates, lipids, and total protein amounts.**

606 Five samples of powder (250 mg each) were pooled for biochemical analyses (1 pool of 5  
 607 individuals per bag). Analyses were done in technical triplicates and data are means  $\pm$  SE (n=  
 608 1 pool x 3 bags x 3 bathymetric levels). 50 mg of nitrogen powder was homogenized in 2 ml  
 609 of nanopure water using a Polytron® PT 2500 E (Kinematica, Luzernerstrasse, Switzerland),  
 610 diluted 10 times and carbohydrate concentration was determined by a colorimetric method  
 611 (DuBois et al., 1956) using a standard calibration curve. Neutral and polar lipids class were  
 612 determined with a CAMAG automatic sampler (CAMAG, Moirans, France) after extraction  
 613 with 200 mg of powder added to 4 ml chloroform-methanol (2:1, v/v; Folch et al., 1957).  
 614 Total protein extraction was done on 450 mg of powder homogenized with a Polytron® PT  
 615 2500 E (Kinematica, Malters, Switzerland) in 5 mL of lysis buffer (Guévelou et al., 2013).  
 616 Total protein content in each lysate was analyzed using the DC protein assay (Bio-Rad) in 96-  
 617 well microplates (Nunc™) using a microplate reader (Bio-Tek®Synergy™ HT, Thermo  
 618 Fisher Scientific, Les Ulis, France). Total protein concentration was obtained using Gen5  
 619 version 2.03 software (Bio-Tek).

	Carbohydrates ( $\mu\text{g}/\text{mg}$ flesh)	Triacylglycerol/sterol (arbitrary unit)	Protein ( $\mu\text{g}/\text{ml}$ flesh)
High (5 m)	$55,16 \pm 7,11$	$4,43 \pm 0,41$	$51,99 \pm 7,51$
Middle (3 m)	$51,32 \pm 3,14$	$5,76 \pm 0,48$	$51,41 \pm 1,58$
Low (1.6 m)	$60,66 \pm 17,77$	$5,83 \pm 1,18$	$40,99 \pm 11,59$



620

621

## 622 AUTHOR CONTRIBUTIONS

623 **C. Corporeau:** Conceptualization, Funding acquisition, Investigation, Methodology, Project  
 624 administration, Supervision, Validation, Roles/Writing-original draft, Writing-review and  
 625 editing; **S. Petton:** Data curation, Visualization; **R. Vilaça:** Formal analysis, Roles/Writing-  
 626 original draft; **L. Delisle:** Formal analysis, Investigation, Methodology, Roles/Writing-review  
 627 and editing; **C. Quééré:** Investigation, Methodology. **V. Le Roy:** Investigation; **C. Dubreuil:**  
 628 Investigation; **S. Lacas-Gervais:** Investigation, Methodology; **Y. Guitton:** Formal analysis,  
 629 Investigation, Methodology; **S. Artigaud:** Formal analysis, Investigation, Validation; **B.**  
 630 **Bernay:** Data curation, Formal analysis, Investigation, Methodology; **V. Pichereau;** Funding  
 631 acquisition, Roles/Writing-review and editing; **A. Huvet:** Formal analysis, Roles/Writing-  
 632 original draft, Writing-review and editing; **B. Petton:** Conceptualization, Methodology,  
 633 Roles/Writing-original draft; **F. Pernet:** Formal analysis, Validation; **E. Fleury:** Formal  
 634 analysis, Roles/Writing-review and editing; **S. Madec:** Roles/ Writing-review and editing; **C.**  
 635 **Brigaudeau:** Conceptualization, Investigation, Roles/Writing-review and editing; **C.**  
 636 **Brenner:** Conceptualization, Funding acquisition, Supervision, Validation, Roles/Writing-  
 637 original draft; **N. Mazure:** Conceptualization, Funding acquisition, Supervision, Validation,  
 638 Roles/Writing-original draft.

## 639 ACKNOWLEDGMENTS

640 This work was supported by Labex Mer (BODY project), the “Fondation ARC pour la  
 641 recherche sur le cancer” (MOLLUSC project), and the ECOSCOPA network founded by the  
 642 French Ministry of the DPMA. We acknowledge the Ifremer staff at Ifremer Argenton and  
 643 Bouin and Fanny Langlois for technical help in biochemistry, University’s CCMA Electron  
 644 Microscopy facility (supported by Université de Nice Sophia- Antipolis, Region Sud Est  
 645 Provence Alpes- Cote d’Azur, Conseil Départemental 06, and Gis Ibis) and Alyssia Marie  
 646 for technical help in microscopy. We thank the Biogenouest-Corsaire core facility for

647 metabolome analyses done with the instrumental facilities LABERCA. We thank Morgan  
648 Smits from Lemar for the English revision of the text.

## 649 7. REFERENCES

- 650 Alfaro, A.C., Young, T., 2018. Showcasing metabolomic applications in aquaculture: a review. *Reviews*  
651 *in Aquaculture* 10, 135–152. <https://doi.org/10.1111/raq.12152>
- 652 Azéma, P., Maurouard, E., Lamy, J.-B., Dégremont, L., 2017. The use of size and growing height to  
653 improve *Crassostrea gigas* farming and breeding techniques against OsHV-1. *Aquaculture*  
654 471, 121–129. <https://doi.org/10.1016/j.aquaculture.2017.01.011>
- 655 Bayne, B.L., 2017. Metabolic Expenditure, in: *Developments in Aquaculture and Fisheries Science*.  
656 Elsevier, pp. 331–415. <https://doi.org/10.1016/B978-0-12-803472-9.00006-6>
- 657 Boltaña, S., Rey, S., Roher, N., Vargas, R., Huerta, M., Huntingford, F.A., Goetz, F.W., Moore, J.,  
658 Garcia-Valtanen, P., Estepa, A., MacKenzie, S., 2013. Behavioural fever is a synergic signal  
659 amplifying the innate immune response. *Proc Biol Sci* 280.  
660 <https://doi.org/10.1098/rspb.2013.1381>
- 661 Cesbron, N., Royer, A.-L., Guitton, Y., Sydor, A., Le Bizec, B., Dervilly-Pinel, G., 2017. Optimization of  
662 fecal sample preparation for untargeted LC-HRMS based metabolomics. *Metabolomics* 13,  
663 99. <https://doi.org/10.1007/s11306-017-1233-8>
- 664 Chawsheen, H.A., Ying, Q., Jiang, H., Wei, Q., 2018. A critical role of the thioredoxin domain  
665 containing protein 5 (TXNDC5) in redox homeostasis and cancer development. *Genes &*  
666 *Diseases* 5, 312–322. <https://doi.org/10.1016/j.gendis.2018.09.003>
- 667 Chen, I.-T., Aoki, T., Huang, Y.-T., Hirono, I., Chen, T.-C., Huang, J.-Y., Chang, G.-D., Lo, C.-F., Wang, H.-  
668 C., 2011. White Spot Syndrome Virus Induces Metabolic Changes Resembling the Warburg  
669 Effect in Shrimp Hemocytes in the Early Stage of Infection. *J. Virol.* 85, 12919–12928.  
670 <https://doi.org/10.1128/JVI.05385-11>
- 671 Corporeau, C., Huvet, A., Pichereau, V., Delisle, L., Quéré, C., Dubreuil, C., Artigaud, S., Brenner, C.,  
672 Meyenberg Cunha-De Padua, M., Mazure, N., 2019. *Crassostrea gigas*, une huître au service  
673 de la recherche sur le cancer. *médecine/sciences* 35, 463–466.  
674 <https://doi.org/10.1051/medsci/2019079>
- 675 Corporeau, C., Tamayo, D., Pernet, F., Quéré, C., Madec, S., 2014. Proteomic signatures of the oyster  
676 metabolic response to herpesvirus OsHV-1  $\mu$ Var infection. *J Proteomics* 109, 176–187.  
677 <https://doi.org/10.1016/j.jprot.2014.06.030>
- 678 de Lorgeril, J., Lucasson, A., Petton, B., Toulza, E., Montagnani, C., Clerissi, C., Vidal-Dupiol, J.,  
679 Chaparro, C., Galinier, R., Escoubas, J.-M., Haffner, P., Dégremont, L., Charrière, G.M., Lafont,  
680 M., Delort, A., Vergnes, A., Chiarello, M., Faury, N., Rubio, T., Leroy, M.A., Pérignon, A.,  
681 Régler, D., Morga, B., Alunno-Bruscia, M., Boudry, P., Le Roux, F., Destoumieux-Garzón, D.,  
682 Gueguen, Y., Mitta, G., 2018. Immune-suppression by OsHV-1 viral infection causes fatal  
683 bacteraemia in Pacific oysters. *Nat Commun* 9, 4215. <https://doi.org/10.1038/s41467-018-06659-3>
- 684
- 685 Delisle, L., Pauletto, M., Vidal-Dupiol, J., Petton, B., Bargelloni, L., Montagnani, C., Pernet, F.,  
686 Corporeau, C., Fleury, E., 2020. High temperature induces transcriptomic changes in  
687 *Crassostrea gigas* that hinders progress of Ostreid herpesvirus (OsHV-1) and promotes  
688 survival. *J Exp Biol* jeb.226233. <https://doi.org/10.1242/jeb.226233>
- 689 Delisle, L., Petton, B., Burguin, J.F., Morga, B., Corporeau, C., Pernet, F., 2018. Temperature modulate  
690 disease susceptibility of the Pacific oyster *Crassostrea gigas* and virulence of the Ostreid  
691 herpesvirus type 1. *Fish Shellfish Immunol.* 80, 71–79.  
692 <https://doi.org/10.1016/j.fsi.2018.05.056>
- 693 Domínguez-Andrés, J., Novakovic, B., Li, Y., Scicluna, B.P., Gresnigt, M.S., Arts, R.J.W., Oosting, M.,  
694 Moorlag, S.J.C.F.M., Groh, L.A., Zwaag, J., Koch, R.M., Horst, R. ter, Joosten, L.A.B., Wijmenga,  
695 C., Michelucci, A., Poll, T. van der, Kox, M., Pickkers, P., Kumar, V., Stunnenberg, H., Netea,  
696 M.G., 2019. The Itaconate Pathway Is a Central Regulatory Node Linking Innate Immune

697 Tolerance and Trained Immunity. *Cell Metabolism* 29, 211-220.e5.  
698 <https://doi.org/10.1016/j.cmet.2018.09.003>

699 Donaghy, L., Artigaud, S., Sussarellu, R., Lambert, C., Le Goïc, N., Hégaret, H., Soudant, P., 2013.  
700 Tolerance of bivalve mollusc hemocytes to variable oxygen availability: a mitochondrial  
701 origin? *Aquatic Living Resources* 26, 257–261. <https://doi.org/10.1051/alr/2013054>

702 DuBois, M., Gilles, K.A., Hamilton, J.K., Rebers, P.A., Smith, F., 1956. Colorimetric Method for  
703 Determination of Sugars and Related Substances 2, 7.

704 Epelboin, Y., Quintric, L., Guévelou, E., Boudry, P., Pichereau, V., Corporeau, C., 2016. The Kinome of  
705 Pacific Oyster *Crassostrea gigas*, Its Expression during Development and in Response to  
706 Environmental Factors. *PLOS ONE* 11, e0155435.  
707 <https://doi.org/10.1371/journal.pone.0155435>

708 Falfushynska, H., Piontkivska, H., Sokolova, I.M., 2020. Effects of intermittent hypoxia on the cell  
709 survival and inflammatory responses in the intertidal marine bivalves *Mytilus edulis* and  
710 *Crassostrea gigas*. *Journal of Experimental Biology*. <https://doi.org/10.1242/jeb.217026>

711 Fleury, E., Barbier, P., Petton, B., Normand, J., Thomas, Y., Pouvreau, S., Daigle, G., Pernet, F., 2020.  
712 Latitudinal drivers of oyster mortality: deciphering host, pathogen and environmental risk  
713 factors. *Scientific Reports* 10, 7264. <https://doi.org/10.1038/s41598-020-64086-1>

714 Fleury, E., Normand, J., Lamoureux, A., Bouget, J.-F., Lupo, C., Cochenec-Laureau, N., Petton, S.,  
715 Petton, B., Pouvreau, S., 2021. RESCO REMORA Database : National monitoring network of  
716 mortality and growth rates of the sentinel oyster *Crassostrea gigas*.  
717 <https://doi.org/10.17882/53007>

718 Folch, J., Lees, M., Stanley, G.H.S., 1957. A SIMPLE METHOD FOR THE ISOLATION AND PURIFICATION  
719 OF TOTAL LIPIDES FROM ANIMAL TISSUES. *Journal of Biological Chemistry* 226, 497–509.  
720 [https://doi.org/10.1016/S0021-9258\(18\)64849-5](https://doi.org/10.1016/S0021-9258(18)64849-5)

721 Fouad, Y.A., Aanei, C., 2017. Revisiting the hallmarks of cancer. *Am J Cancer Res* 7, 1016–1036.

722 Galenza, A., Foley, E., 2019. Immunometabolism: Insights from the *Drosophila* model. *Developmental*  
723 *& Comparative Immunology* 94, 22–34. <https://doi.org/10.1016/j.dci.2019.01.011>

724 Green, T.J., Robinson, N., Chataway, T., Benkendorff, K., O'Connor, W., Speck, P., 2014. Evidence that  
725 the major hemolymph protein of the Pacific oyster, *Crassostrea gigas*, has antiviral activity  
726 against herpesviruses. *Antiviral Research* 110, 168–174.  
727 <https://doi.org/10.1016/j.antiviral.2014.08.010>

728 Guévelou, E., Huvet, A., Sussarellu, R., Milan, M., Guo, X., Li, L., Zhang, G., Quillien, V., Daniel, J.-Y.,  
729 Quéré, C., Boudry, P., Corporeau, C., 2013. Regulation of a truncated isoform of AMP-  
730 activated protein kinase  $\alpha$  (AMPK $\alpha$ ) in response to hypoxia in the muscle of Pacific oyster  
731 *Crassostrea gigas*. *J. Comp. Physiol. B, Biochem. Syst. Environ. Physiol.* 183, 597–611.  
732 <https://doi.org/10.1007/s00360-013-0743-6>

733 He, S., Song, L., Qian, Z., Hou, F., Liu, Y., Wang, X., Peng, Z., Sun, C., Liu, X., 2015. Molecular  
734 characterization of LvAV in response to white spot syndrome virus infection in the pacific  
735 white shrimp (*Litopenaeus vannamei*). *Dev. Comp. Immunol.* 51, 48–55.  
736 <https://doi.org/10.1016/j.dci.2015.02.020>

737 Hooftman, A., O'Neill, L.A.J., 2019. The Immunomodulatory Potential of the Metabolite Itaconate.  
738 *Trends Immunol* 40, 687–698. <https://doi.org/10.1016/j.it.2019.05.007>

739 Itoh, N., Xue, Q.-G., Schey, K.L., Li, Y., Cooper, R.K., La Peyre, J.F., 2011. Characterization of the major  
740 plasma protein of the eastern oyster, *Crassostrea virginica*, and a proposed role in host  
741 defense. *Comp. Biochem. Physiol. B-Biochem. Mol. Biol.* 158, 9–22.  
742 <https://doi.org/10.1016/j.cbpb.2010.06.006>

743 Jenkins, D., 2008. Role for Major Vault Protein in the innate immunity of respiratory epithelium.  
744 *Thorax* 63, 107–107.

745 Jia, X., Wang, F., Lu, Y., Zhang, D., Dong, S., 2014. Immune responses of *Litopenaeus vannamei* to  
746 thermal stress: a comparative study of shrimp in freshwater and seawater conditions. *Marine*  
747 *and Freshwater Behaviour and Physiology* 47, 79–92.  
748 <https://doi.org/10.1080/10236244.2014.894349>

749 Jia, Z., Jiang, S., Wang, M., Wang, X., Liu, Y., Lv, Z., Song, X., Li, Y., Wang, L., Song, L., 2021.  
750 Identification of a Novel Pattern Recognition Receptor DM9 Domain Containing Protein 4 as  
751 a Marker for Pro-Hemocyte of Pacific Oyster *Crassostrea gigas*. *Frontiers in Immunology* 11,  
752 3811. <https://doi.org/10.3389/fimmu.2020.603270>

753 Kanost, M.R., 1999. Serine proteinase inhibitors in arthropod immunity. *Developmental &*  
754 *Comparative Immunology, Invertebrate Immunity* 23, 291–301.  
755 [https://doi.org/10.1016/S0145-305X\(99\)00012-9](https://doi.org/10.1016/S0145-305X(99)00012-9)

756 Keating, S.T., El-Osta, A., 2015. Epigenetics and metabolism. *Circ. Res.* 116, 715–736.  
757 <https://doi.org/10.1161/CIRCRESAHA.116.303936>

758 Lafont, M., Vergnes, A., Vidal-Dupiol, J., de Lorgeril, J., Gueguen, Y., Haffner, P., Petton, B., Chaparro,  
759 C., Barrachina, C., Destoumieux-Garzon, D., Mitta, G., Gourbal, B., Montagnani, C., 2020. A  
760 Sustained Immune Response Supports Long-Term Antiviral Immune Priming in the Pacific  
761 Oyster, *Crassostrea gigas*. *mBio* 11, e02777-19, /mbio/11/2/mBio.02777-19.atom.  
762 <https://doi.org/10.1128/mBio.02777-19>

763 Li, L., Li, A., Song, K., Meng, J., Guo, X., Li, S., Li, C., De Wit, P., Que, H., Wu, F., Wang, W., Qi, H., Xu, F.,  
764 Cong, R., Huang, B., Li, Y., Wang, T., Tang, X., Liu, S., Li, B., Shi, R., Liu, Y., Bu, C., Zhang, C., He,  
765 W., Zhao, S., Li, H., Zhang, S., Zhang, L., Zhang, G., 2018. Divergence and plasticity shape  
766 adaptive potential of the Pacific oyster. *Nat Ecol Evol* 2, 1751–1760.  
767 <https://doi.org/10.1038/s41559-018-0668-2>

768 Liao, S.-T., Han, C., Xu, D.-Q., Fu, X.-W., Wang, J.-S., Kong, L.-Y., 2019. 4-Octyl itaconate inhibits  
769 aerobic glycolysis by targeting GAPDH to exert anti-inflammatory effects. *Nature*  
770 *Communications* 10, 5091. <https://doi.org/10.1038/s41467-019-13078-5>

771 LIN, D.Y., WEI, L.J., YING, Z., 1993. Checking the Cox model with cumulative sums of martingale-based  
772 residuals. *Biometrika* 80, 557–572. <https://doi.org/10.1093/biomet/80.3.557>

773 Livak, K.J., Schmittgen, T.D., 2001. Analysis of Relative Gene Expression Data Using Real-Time  
774 Quantitative PCR and the 2- $\Delta\Delta$ CT Method. *Methods* 25, 402–408.  
775 <https://doi.org/10.1006/meth.2001.1262>

776 Mazaleyrat, A., Normand, J., Dubroca, L., Fleury, E., 2022. A 26-year time series of mortality and  
777 growth of the Pacific oyster *C. gigas* recorded along French coasts. *Sci Data* 9, 392.  
778 <https://doi.org/10.1038/s41597-022-01511-2>

779 Melillo, D., Marino, R., Italiani, P., Boraschi, D., 2018. Innate Immune Memory in Invertebrate  
780 Metazoans: A Critical Appraisal. *Front Immunol* 9.  
781 <https://doi.org/10.3389/fimmu.2018.01915>

782 Meng, J., Wang, T., Li, L., Zhang, G., 2018. Inducible variation in anaerobic energy metabolism reflects  
783 hypoxia tolerance across the intertidal and subtidal distribution of the Pacific oyster  
784 (*Crassostrea gigas*). *Mar Environ Res* 138, 135–143.  
785 <https://doi.org/10.1016/j.marenvres.2018.04.002>

786 Mills, E.L., Ryan, D.G., Prag, H.A., Dikovskaya, D., Menon, D., Zaslon, Z., Jedrychowski, M.P., Costa,  
787 A.S.H., Higgins, M., Hams, E., Szpyt, J., Runtsch, M.C., King, M.S., McGouran, J.F., Fischer, R.,  
788 Kessler, B.M., McGettrick, A.F., Hughes, M.M., Carroll, R.G., Booty, L.M., Knatko, E.V.,  
789 Meakin, P.J., Ashford, M.L.J., Modis, L.K., Brunori, G., Sévin, D.C., Fallon, P.G., Caldwell, S.T.,  
790 Kunji, E.R.S., Chouchani, E.T., Frezza, C., Dinkova-Kostova, A.T., Hartley, R.C., Murphy, M.P.,  
791 O’Neill, L.A., 2018. Itaconate is an anti-inflammatory metabolite that activates Nrf2 via  
792 alkylation of KEAP1. *Nature* 556, 113–117. <https://doi.org/10.1038/nature25986>

793 Morga, B., Faury, N., Guesdon, S., Chollet, B., Renault, T., 2017. Haemocytes from *Crassostrea gigas*  
794 and OsHV-1: A promising in vitro system to study host/virus interactions. *Journal of*  
795 *Invertebrate Pathology* 150, 45–53. <https://doi.org/10.1016/j.jip.2017.09.007>

796 Netea, M.G., Domínguez-Andrés, J., Barreiro, L.B., Chavakis, T., Divangahi, M., Fuchs, E., Joosten,  
797 L.A.B., van der Meer, J.W.M., Mhlanga, M.M., Mulder, W.J.M., Riksen, N.P., Schlitzer, A.,  
798 Schultze, J.L., Stabel Benn, C., Sun, J.C., Xavier, R.J., Latz, E., 2020. Defining trained immunity  
799 and its role in health and disease. *Nature Reviews Immunology* 20, 375–388.  
800 <https://doi.org/10.1038/s41577-020-0285-6>

801 Nguyen, T.V., Alfaro, A.C., Merien, F., Young, T., Grandiosa, R., 2018. Metabolic and immunological  
802 responses of male and female new Zealand Greenshell™ mussels (*Perna canaliculus*) infected  
803 with *Vibrio* sp. *Journal of Invertebrate Pathology* 157, 80–89.  
804 <https://doi.org/10.1016/j.jip.2018.08.008>

805 Nguyen, T.V., Alfaro, A.C., Young, T., Green, S., Zarate, E., Merien, F., 2019. Itaconic acid inhibits  
806 growth of a pathogenic marine *Vibrio* strain: A metabolomics approach. *Scientific Reports* 9,  
807 5937. <https://doi.org/10.1038/s41598-019-42315-6>

808 Offret, C., Paulino, S., Gauthier, O., Château, K., Bidault, A., Corporeau, C., Miner, P., Petton, B.,  
809 Pernet, F., Fabioux, C., Paillard, C., Blay, G.L., 2020. The marine intertidal zone shapes oyster  
810 and clam digestive bacterial microbiota. *FEMS Microbiol Ecol* 96, 1–12.  
811 <https://doi.org/10.1093/femsec/fiaa078>

812 O’Neill, L.A.J., Artyomov, M.N., 2019. Itaconate: the poster child of metabolic reprogramming in  
813 macrophage function. *Nature Reviews Immunology* 19, 273–281.  
814 <https://doi.org/10.1038/s41577-019-0128-5>

815 O’Neill, L.A.J., Kishton, R.J., Rathmell, J., 2016. A guide to immunometabolism for immunologists. *Nat*  
816 *Rev Immunol* 16, 553–565. <https://doi.org/10.1038/nri.2016.70>

817 Ottaviani, E., Malagoli, D., Grimaldi, A., Eguileor, M. de, 2012. The immunoregulator role of neprilysin  
818 (NEP) in invertebrates. *ISJ-INVERT SURVIV J* 9, 207–211.

819 Pauletto, M., Segarra, A., Montagnani, C., Quillien, V., Faury, N., Le Grand, J., Miner, P., Petton, B.,  
820 Labreuche, Y., Fleury, E., Fabioux, C., Bargelloni, L., Renault, T., Huvet, A., 2017. Long dsRNAs  
821 promote an anti-viral response in Pacific oyster hampering ostreid herpesvirus 1 replication. *J*  
822 *Exp Biol* 220, 3671–3685. <https://doi.org/10.1242/jeb.156299>

823 Pepin, J.F., Riou, A., Renault, T., 2008. Rapid and sensitive detection of ostreid herpesvirus 1 in oyster  
824 samples by real-time PCR. *Journal of Virological Methods* 149, 269–276.  
825 <https://doi.org/10.1016/j.jviromet.2008.01.022>

826 Perez-Riverol, Y., Csordas, A., Bai, J., Bernal-Llinares, M., Hewapathirana, S., Kundu, D.J., Inuganti, A.,  
827 Griss, J., Mayer, G., Eisenacher, M., Pérez, E., Uszkoreit, J., Pfeuffer, J., Sachsenberg, T.,  
828 Yilmaz, S., Tiwary, S., Cox, J., Audain, E., Walzer, M., Jarnuczak, A.F., Ternent, T., Brazma, A.,  
829 Vizcaíno, J.A., 2019. The PRIDE database and related tools and resources in 2019: improving  
830 support for quantification data. *Nucleic Acids Res* 47, D442–D450.  
831 <https://doi.org/10.1093/nar/gky1106>

832 Pernet, F., Barret, J., Dégremont, L., Lagarde, F., Pépin, J.-F., Keck, N., 2012. Mass mortalities of  
833 Pacific oysters *Crassostrea gigas* reflect infectious diseases and vary with farming practices in  
834 the Mediterranean Thau lagoon, France 23.

835 Pernet, F., Fuhrmann, M., Petton, B., Mazurié, J., Bouget, J.-F., Fleury, E., Daigle, G., Gernez, P., 2018.  
836 Determination of risk factors for herpesvirus outbreak in oysters using a broad-scale spatial  
837 epidemiology framework. *Scientific Reports* 8. <https://doi.org/10.1038/s41598-018-29238-4>

838 Pernet, F., Gachelin, S., Stanisière, J.-Y., Petton, B., Fleury, E., Mazurié, J., 2019. Farmer monitoring  
839 reveals the effect of tidal height on mortality risk of oysters during a herpesvirus outbreak.  
840 *ICES J Mar Sci* 76, 1816–1824. <https://doi.org/10.1093/icesjms/fsz074>

841 Petton, B., Boudry, P., Alunno-Bruscia, M., Pernet, F., 2015. Factors influencing disease-induced  
842 mortality of Pacific oysters *Crassostrea gigas*. *Aquaculture Environment Interactions* 6, 205–  
843 222. <https://doi.org/10.3354/aei00125>

844 Petton, S., Corporeau, C., Quemener, L., 2020. Temperature monitoring of subtidal and intertidal  
845 microhabitats of oyster *Crassostrea gigas*. SEANO data set. <https://doi.org/10.17882/79095>

846 Phupet, B., Pitakpornprecha, T., Baowubon, N., Runsaeng, P., Utarabhand, P., 2018.  
847 Lipopolysaccharide- and  $\beta$ -1,3-glucan-binding protein from *Litopenaeus vannamei*:  
848 Purification, cloning and contribution in shrimp defense immunity via phenoloxidase  
849 activation. *Developmental & Comparative Immunology* 81, 167–179.  
850 <https://doi.org/10.1016/j.dci.2017.11.016>

851 Rosani, U., Young, T., Bai, C.-M., Alfaro, A.C., Venier, P., 2019. Dual Analysis of Virus-Host  
852 Interactions: The Case of *Ostreid herpesvirus 1* and the Cupped Oyster *Crassostrea gigas*. *Evol*  
853 *Bioinform Online* 15, 117693431983130. <https://doi.org/10.1177/1176934319831305>

854 Rozenn Cannuel, P.G.B., 2005. Is oyster broodstock feeding always necessary? A study using oocyte  
855 quality predictors and validators in *Crassostrea gigas*. *Aquat Living Resour* 18, 35–43.  
856 <https://doi.org/10.1051/alr:2005003>

857 Rybakin, V., Clemen, C.S., 2005. Coronin proteins as multifunctional regulators of the cytoskeleton  
858 and membrane trafficking. *BioEssays* 27, 625–632. <https://doi.org/10.1002/bies.20235>

859 Sanchez, E.L., Lagunoff, M., 2015. Viral activation of cellular metabolism. *Virology*, 60th Anniversary  
860 Issue 479–480, 609–618. <https://doi.org/10.1016/j.virol.2015.02.038>

861 Scanes, E., Parker, L.M., O'Connor, W.A., Stapp, L.S., Ross, P.M., 2017. Intertidal oysters reach their  
862 physiological limit in a future high-CO<sub>2</sub> world. *J Exp Biol* 220, 765–774.  
863 <https://doi.org/10.1242/jeb.151365>

864 Scotti, P.D., Dearing, S.C., Greenwood, D.R., 2007. Characterisation of cavortin, the major  
865 haemolymph protein of the Pacific oyster (*Crassostrea gigas*). *New Zealand Journal of Marine*  
866 *and Freshwater Research* 41, 91–101. <https://doi.org/10.1080/00288330709509898>

867 Segarra, A., Faury, N., Pépin, J.-F., Renault, T., 2014. Transcriptomic study of 39 ostreid herpesvirus 1  
868 genes during an experimental infection. *Journal of Invertebrate Pathology* 119, 5–11.  
869 <https://doi.org/10.1016/j.jip.2014.03.002>

870 Sokolov, E.P., Markert, S., Hinzke, T., Hirschfeld, C., Becher, D., Ponsuksili, S., Sokolova, I.M., 2019.  
871 Effects of hypoxia-reoxygenation stress on mitochondrial proteome and bioenergetics of the  
872 hypoxia-tolerant marine bivalve *Crassostrea gigas*. *Journal of Proteomics* 194, 99–111.  
873 <https://doi.org/10.1016/j.jprot.2018.12.009>

874 Sokolova, I., 2018. Mitochondrial Adaptations to Variable Environments and Their Role in Animals'  
875 Stress Tolerance. *Integrative and Comparative Biology* 58, 519–531.  
876 <https://doi.org/10.1093/icb/icy017>

877 Su, M.-A., Huang, Y.-T., Chen, I.-T., Lee, D.-Y., Hsieh, Y.-C., Li, C.-Y., Ng, T.H., Liang, S.-Y., Lin, S.-Y.,  
878 Huang, S.-W., Chiang, Y.-A., Yu, H.-T., Khoo, K.-H., Chang, G.-D., Lo, C.-F., Wang, H.-C., 2014.  
879 An invertebrate Warburg effect: a shrimp virus achieves successful replication by altering the  
880 host metabolome via the PI3K-Akt-mTOR pathway. *PLoS Pathog.* 10, e1004196.  
881 <https://doi.org/10.1371/journal.ppat.1004196>

882 Sussarellu, R., Dudognon, T., Fabioux, C., Soudant, P., Moraga, D., Kraffe, E., 2013. Rapid  
883 mitochondrial adjustments in response to short-term hypoxia and re-oxygenation in the  
884 Pacific oyster, *Crassostrea gigas*. *Journal of Experimental Biology* 216, 1561–1569.  
885 <https://doi.org/10.1242/jeb.075879>

886 Sussarellu, R., Fabioux, C., Camacho Sanchez, M., Le Goïc, N., Lambert, C., Soudant, P., Moraga, D.,  
887 2012. Molecular and cellular response to short-term oxygen variations in the Pacific oyster  
888 *Crassostrea gigas*. *Journal of Experimental Marine Biology and Ecology* 412, 87–95.  
889 <https://doi.org/10.1016/j.jembe.2011.11.007>

890 Sussarellu, R., Suquet, M., Thomas, Y., Lambert, C., Fabioux, C., Pernet, M.E.J., Le Goic, N., Quillien,  
891 V., Mingant, C., Epelboin, Y., Corporeau, C., Guyomarch, J., Robbens, J., Paul-Pont, I.,  
892 Soudant, P., Huvet, A., 2016. Oyster reproduction is affected by exposure to polystyrene  
893 microplastics. *Proceedings Of The National Academy Of Sciences Of The United States Of*  
894 *America* 113, 2430–2435. <https://doi.org/10.1073/pnas.1519019113>

895 Talwar, C., Nagar, S., Lal, R., Negi, R.K., 2018. Fish Gut Microbiome: Current Approaches and Future  
896 Perspectives. *Indian J Microbiol* 58, 397–414. <https://doi.org/10.1007/s12088-018-0760-y>

897 Tkaczuk, K.L., A Shumilin, I., Chruszcz, M., Evdokimova, E., Savchenko, A., Minor, W., 2013. Structural  
898 and functional insight into the universal stress protein family. *Evol Appl* 6, 434–449.  
899 <https://doi.org/10.1111/eva.12057>

900 Van Nguyen, T., Alfaro, A.C., 2019. Targeted metabolomics to investigate antimicrobial activity of  
901 itaconic acid in marine molluscs. *Metabolomics* 15, 97. <https://doi.org/10.1007/s11306-019-1556-8>

902

903 Vollmer, A.C., Bark, S.J., 2018. Twenty-Five Years of Investigating the Universal Stress Protein:  
 904 Function, Structure, and Applications. *Adv Appl Microbiol* 102, 1–36.  
 905 <https://doi.org/10.1016/bs.aambs.2017.10.001>

906 Wang, Z., Liu, D., Varin, A., Nicolas, V., Courilleau, D., Mateo, P., Caubere, C., Rouet, P., Gomez, A.-M.,  
 907 Vandecasteele, G., Fischmeister, R., Brenner, C., 2016. A cardiac mitochondrial cAMP  
 908 signaling pathway regulates calcium accumulation, permeability transition and cell death.  
 909 *Cell Death & Disease* 7, e2198–e2198. <https://doi.org/10.1038/cddis.2016.106>

910 Warburg, O., 1956. On the origin of cancer cells. *Science* 123, 309–314.

911 Watanabe, Y., Tateno, H., Nakamura-Tsuruta, S., Kominami, J., Hirabayashi, J., Nakamura, O.,  
 912 Watanabe, T., Kamiya, H., Naganuma, T., Ogawa, T., Naudé, R.J., Muramoto, K., 2009. The  
 913 function of rhamnose-binding lectin in innate immunity by restricted binding to Gb3. *Dev*  
 914 *Comp Immunol* 33, 187–197. <https://doi.org/10.1016/j.dci.2008.08.008>

915 Webb, S.C., Fidler, A., Renault, T., 2007. Primers for PCR-based detection of ostreid herpes virus-1  
 916 (OsHV-1): Application in a survey of New Zealand molluscs. *Aquaculture* 272, 126–139.  
 917 <https://doi.org/10.1016/j.aquaculture.2007.07.224>

918 Whyte, J.N.C., Englar, J.R., Carswell, B.L., 1990. Biochemical composition and energy reserves in  
 919 *Crassostrea gigas* exposed to different levels of nutrition. *Aquaculture* 90, 157–172.  
 920 [https://doi.org/10.1016/0044-8486\(90\)90338-N](https://doi.org/10.1016/0044-8486(90)90338-N)

921 Yang, M.-J., Song, H., Yu, Z.-L., Xu, T., Hu, Z., Zhou, C., Shi, P., Zhang, T., 2020. Identification and  
 922 expression characterization of a novel carboxypeptidase A-like gene (RvCPA) during early  
 923 developmental stages in the gastropod *Rapana venosa* (Muricidae). *Aquaculture Reports* 17,  
 924 100360. <https://doi.org/10.1016/j.aqrep.2020.100360>

925 Young, T., Kesarcodi-Watson, A., Alfaro, A.C., Merien, F., Nguyen, T.V., Mae, H., Le, D.V., Villas-Bôas,  
 926 S., 2017. Differential expression of novel metabolic and immunological biomarkers in oysters  
 927 challenged with a virulent strain of OsHV-1. *Dev. Comp. Immunol.* 73, 229–245.  
 928 <https://doi.org/10.1016/j.dci.2017.03.025>

929 Zacchi, L.F., Selmecki, A.M., Berman, J., Davis, D.A., 2010. Low Dosage of Histone H4 Leads to Growth  
 930 Defects and Morphological Changes in *Candida albicans*. *PLoS ONE* 5, e10629.  
 931 <https://doi.org/10.1371/journal.pone.0010629>

932 Zhang, Guofan, Fang, X., Guo, X., Li, L., Luo, R., Xu, F., Yang, P., Zhang, L., Wang, X., Qi, H., Xiong, Z.,  
 933 Que, H., Xie, Y., Holland, P.W.H., Paps, J., Zhu, Y., Wu, F., Chen, Y., Wang, Jiafeng, Peng, C.,  
 934 Meng, J., Yang, L., Liu, J., Wen, B., Zhang, N., Huang, Z., Zhu, Q., Feng, Y., Mount, A.,  
 935 Hedgecock, D., Xu, Z., Liu, Y., Domazet-Lošo, T., Du, Y., Sun, X., Zhang, Shoudu, Liu, B., Cheng,  
 936 P., Jiang, X., Li, J., Fan, D., Wang, W., Fu, W., Wang, T., Wang, B., Zhang, J., Peng, Z., Li,  
 937 Yingxiang, Li, Na, Wang, Jinpeng, Chen, M., He, Y., Tan, F., Song, X., Zheng, Q., Huang, R.,  
 938 Yang, Hailong, Du, X., Chen, L., Yang, M., Gaffney, P.M., Wang, S., Luo, L., She, Z., Ming, Y.,  
 939 Huang, W., Zhang, Shu, Huang, B., Zhang, Y., Qu, T., Ni, P., Miao, G., Wang, Junyi, Wang, Q.,  
 940 Steinberg, C.E.W., Wang, H., Li, Ning, Qian, L., Zhang, Guojie, Li, Yingrui, Yang, Huanming, Liu,  
 941 X., Wang, Jian, Yin, Y., Wang, Jun, 2012. The oyster genome reveals stress adaptation and  
 942 complexity of shell formation. *Nature* 490, 49–54. <https://doi.org/10.1038/nature11413>

943 Zhang, G., Li, L., Meng, J., Qi, H., Qu, T., Xu, F., Zhang, L., 2016. Molecular Basis for Adaptation of  
 944 Oysters to Stressful Marine Intertidal Environments. *Annu Rev Anim Biosci* 4, 357–381.  
 945 <https://doi.org/10.1146/annurev-animal-022114-110903>

946